REVIEWS OF TOPICAL PROBLEMS

Experimental methods for determining the melting temperature and the heat of melting of clusters and nanoparticles

G N Makarov

Contents

Abstract. Unlike macroscopic objects, clusters and nanoparticles lack a definite melting temperature at a given pressure but rather have their solid and liquid phases coexistent in a certain temperature range and their melting temperature dependent on the particle size. As the particle size decreases, the melting temperature becomes fundamentally difficult to define. This review examines methods for measuring the melting temperature and the heat of melting of clusters and nanoparticles. The temperature (internal energy) of the particles is defined and how it affects the properties of and processes involving the particles is discussed. The melting features of clusters and nanoparticles versus bulk materials are examined. Early methods of determining the melting temperature of large clusters are described. New precision methods of measuring the melting temperature and the heat of melting of clusters are discussed, which use the clusters themselves as 'high-sensitivity calorimeters' to measure energy. Laser-based nanoparticle melting techniques are outlined.

G N Makarov Institute of Spectroscopy, Russian Academy of Sciences, ul. Fizicheskaya 5, 142190 Troitsk, Moscow region, Russian Federation
Tel. (7-496) 751 02 32
Fax (7-496) 751 08 86
E-mail: gmakarov@isan.troitsk.ru

1. Introduction

Cluster and nanoparticle studies are currently a central area of research in physics and chemistry (see, for instance, monographs, collected volumes of scientific works, reviews [1 – 46] and references cited therein). V L Ginzburg placed cluster investigations No. 7 in his classification of the most important and interesting problems in physics and astrophysics [47, 48]. The tremendous practical and academic significance of cluster and nanoparticle research is due to unique properties of these structures and their wide application in nanotechnologies [49, 50] for manufacturing high-speed electronic devices and large memory systems, depositing thin films, producing novel materials and developing methods of their surface treatment [1, 23, 27, 37, 39]. Metallic and composite clusters and nanoparticles have recently been attracting increasingly more attention for the possibility of using them in the search for new high-temperature superconducting materials, too [44, 51 – 54]. All these applications imply a good knowledge of the physical, chemical, and thermodynamic properties of clusters and nanoparticles, which are different from the properties of both their constituent particles and bulk materials by virtue of the discrete structure of their energy levels and large surface-to-volume ratios. Such small systems essentially depend on quantum and tunneling effects, as well as structural, dimensional, and surface effects that determine many properties and parameters of clusters and nanoparticles, including their melting temperature and heat of fusion [43]. The melting temperature and heat of fusion of clusters and nanoparticles

are important physical characteristics of great theoretical and applied interest. At the same time, determination of the melting temperature and heat of fusion of clusters and nanoparticles encounter serious difficulties. Unique techniques developed for their measurements are evoking excitement. It is precisely the experimental methods for measuring the melting temperature and heat of fusion of clusters and nanoparticles that are dealt with in the present review.

Clusters and nanoparticles are actually identical aggregates. In his notable book [1], H Pauly describes clusters as aggregates of a few to several millions of atoms or molecules held together by different types of bonds with a binding energy from a few tenths of an electron-volt to several electron-volts. In this broad sense, clusters are small aggregates of atoms and molecules coupled by weak ($\leqslant 0.05-0.2$ eV) van der Waals bonds or stronger ($\approx 0.3-0.6$ eV) hydrogen bonds, as well as aggregates of metal, semiconductor, and carbon atoms with rather strong ($\approx 1-10$ eV) bonding. These aggregates are quite different in terms of structure, type, bond strength, and physical and chemical properties [1, 27, 30, 31, 36, 39, 43]. Nanoparticles are usually defined as small aggregates from 1 to 100 nm (or 10 to 1000 Å) in size [55 – 57]. Let us compare the sizes of clusters and nanoparticles. The radius of a spherical cluster containing N atoms is given by

$$R_N = R_0 N^{1/3}, \tag{1.1}$$

where R_0 is the monomer radius. At $R_0 \approx 2-3$ Å, clusters containing $N \approx 10^7$ and 50 atoms have radii $R_N \approx 400-600$ Å and $R_N \approx 7.5-11$ Å, respectively, meaning that clusters of $50 \leqslant N \leqslant 10^7$ atoms and nanoparticles are identical aggregates. Therefore, we do not distinguish between clusters and nanoparticles later in this review except in considering small clusters ($N \leqslant 10$), which we shall not regard as nanoparticles. Also, it should be emphasized that by nanoparticles are meant aggregates composed of metal, carbon, and semiconductor atoms, as well as of composite materials, i.e., strongly coupled aggregates. At the same time, relatively large clusters of molecular and noble gases, including van der Waals clusters, are also referred to as nanoparticles. The commonness of all these aggregates is confirmed by the fact that the electronic properties and electrical conductivity of small-sized objects (e.g., nanowires and nanocontacts) characterized, similarly to clusters, by the high surface-to-volume ratio, are possible to describe using theoretical models and approaches applicable to the description of clusters [58].

It should be noted that the above definition of the cluster based on the number of its constituent atoms (molecules) does not imply the manifestation of a dimensional effect in these aggregates. It is the size dependences of the physical, chemical, and thermodynamic properties and parameters of clusters, as well as their difference from those of macroscopic substances, that are the major characteristics of clusters.

The review outline is as follows. Section 2 treats cluster (nanoparticle) temperature (internal energy). Kinetic and thermodynamic definitions of the cluster temperature are proposed. Temperature is shown to influence cluster properties and physicochemical processes with the participation of clusters and cluster beams. Temperature values are estimated for clusters produced upon gas expansion without a carrier in a nozzle source. The relationships between cluster temperature and the interaction potential of intracluster atoms

(molecules) and between temperature and vaporization heat are illustrated. The peculiarities of the solid–liquid phase transition in clusters compared with the analogous phase transition in macroscopic systems are considered in Section 3. It contains an analysis of the distinctive features of the phase transition in clusters, such as the coexistence of the two phases and the possibility of occurring negative heat capacity near the melting point. Configuration excitation of clusters as a basis for the solid-liquid phase transition is discussed in qualitative terms.

The central Section 4 is concerned with experimental methods for measuring the melting temperature and heat of fusion of clusters and nanoparticles. Early methods of determination of melting temperature of large clusters are described along with optical and calorimetric methods for measuring temperature and heat of fusion. The size dependence of cluster melting temperature and its relation to the cluster structure are considered. Comprehensive analysis is presented of recently developed sophisticated methods for measuring cluster temperature and heat of fusion in which the clusters themselves are used as 'highly sensitive calorimeters' to measure energy. Laser techniques for the observation of a solid–liquid phase transition in nanoparticles are briefly described. The concluding Section 5 summarizes the main results of the research under discussion; the author's view of the most important achievements in the field of interest and priority areas of further studies are also offered.

2. Cluster (nanoparticle) temperature

2.1 Kinetic and thermodynamic definitions of cluster temperature

Cluster (nanoparticle) temperature depends on the energy of random motion of constituent atoms or molecules with respect to the cluster's center of mass. If rotational and translational degrees of freedom of a cluster are 'frozen', its internal temperature T_{cl} is given by the relation

$$\frac{3N}{2} k_{\mathrm{B}} T_{\mathrm{cl}} = \left\langle \sum_{i=1}^{N} \frac{m_i (v_{\mathrm{cm}} - v_i)^2}{2} \right\rangle, \tag{2.1}$$

where m_i and v_i are the mass and velocity of the cluster's atoms (molecules), v_{cm} is the velocity of the cluster's center of mass, N is the number of particles in the cluster, and k_{B} is the Boltzmann constant.

Relation (2.1) represents the kinetic definition of cluster temperature, which can be just as well defined as the thermodynamic quantity

$$T_{\mathrm{cl}} = \frac{\mathrm{d}E}{\mathrm{d}S}, \tag{2.2}$$

where E and S are the total internal energy and entropy of the cluster, respectively. Generally speaking, temperatures given by relationships (2.1) and (2.2) are different quantities, and this difference may have serious consequences (see Refs [38, 59, 60] and references cited therein). Thermodynamic consideration of clusters takes into account not only the energy of thermal atomic motion but also the potential energy of atom–atom interactions inside the cluster, including the configuration excitation energy. By way of example, for a cluster of N atoms with pairwise interaction, one obtains

$$E = U + K = \sum_{i,j} u(r_{ij}) + \frac{m}{2} \sum_{i} \left(\frac{\mathrm{d}r_i}{\mathrm{d}t} \right)^2. \tag{2.3}$$

Here, U is the total potential energy, K is the total kinetic energy of atoms, $u(r_{ij})$ is the atom–atom interaction potential at a distance $r_{ij} = r_i - r_j$, r_i, r_j are the coordinates of the atoms, and m is the atomic mass. Cluster entropy in this case can be described by the general expression for entropy [61]:

$$S = -\langle \ln P \rangle = -\sum_i P_i \ln P_i, \qquad (2.4)$$

where the subscript i characterizes the cluster state, and P_i is the probability of the cluster being in this state ($\sum_i P_i$) = 1.

By configuration excitation is understood transitions from the cluster's ground state to the local minima of multidimensional space of the potential energy surface. Specifically, it is precisely the configuration excitations that are responsible for changes in cluster structure and the aggregate state [7, 25, 38, 45, 59, 60] (see also Section 3).

Thermodynamic definition of cluster temperature taking into account cluster's total internal energy and entropy makes it possible to describe many processes proceeding at structural transitions and provides a deeper insight into the physics of phase transitions in clusters [7, 38, 45, 60] (see Section 3). By way of example, the thermodynamic consideration has been applied to predict the negative heat capacity of a cluster near the melting point [62–67]. Many authors have examined the negative heat capacity of clusters in experiment [68–73] (see Section 3.3).

The temperature of clusters depends on their type (composition), modes of formation, and stabilization; it varies in a broad range [43]. For example, the temperature of ^{3}He and ^{4}He clusters stabilized in the evaporation process amounts to 0.15 and 0.38 K [74, 75]. The temperature of noble gas clusters obtained either in molecular beams or by aggregation varies as a rule from a few to tens of Kelvin degrees. Molecular clusters (including those with hydrogen bonds) are characterized by a temperature from several dozen to several hundreds of Kelvin degrees. The temperature of metal and carbon clusters (including fullerenes) obtained by laser-aided methods or in discharges may be in the range of 3500–4000 K, and that of high-melting-point materials can be 4500–5000 K. The cluster temperature can grow essentially with heightening the level of excitation of the clusters, e.g., by electron impact [76–80], energetic ions [81, 82], laser radiation [83–89] (including the effect of powerful ultrashort laser pulses [24, 26–29]), and collisions of high-energy clusters and cluster ions with a solid surface [17, 39] or between themselves in counter-propagating beams [90–96] (see recent reviews [39, 43] and references cited therein). Under equilibrium conditions, the cluster upper limiting temperature coincides with the boiling point of the cluster material. In other words, equilibrium temperature of clusters fabricated from carbon and metal atoms, and high-melting-point materials may vary broadly, whereas temperature variations of molecular clusters are much less pronounced and those of noble gas (especially helium) clusters are even smaller.

2.2 Effect of cluster temperature on the properties of clusters and processes involving them

Cluster temperature constitutes an important physical parameter playing a key role in many physicochemical processes involving clusters and cluster beams [43]. The internal temperature of clusters determines their polarizability and magnetic moments, ionization potentials, structure, and optical properties (see Section 4.3). Internal temperature

also influences many other properties of clusters and processes with their participation [97, 98]. Suffice it to say that it is essential for charge transfer in collisions between metal cluster ions and metal atoms [99, 100], which underlie many chemical reactions.

Pathways of cluster and cluster ion fragmentation upon cluster collisions with atoms or a solid surface also depend on temperature [39, 43]. The same is true of cluster energy relaxation mechanisms (fragmentation, emission of electrons, charged particles, and light [39, 43]. As shown by the example of carbon clusters [81, 84], the main energy relaxation channels at temperatures above 3000 K are fragmentation and thermal electron emission, while cluster cooling due to emission of equilibrium radiation prevails at lower temperatures. Cluster temperature significantly affects the rate of reactions between clusters and other reactants [101, 102], as well as rates and channels of reactions proceeding at the surface or inside large ($N \geqslant 10^3$) van der Waals clusters (see, for instance, Refs [103–106]). Of special interest in this context are chemical reactions inside nanodroplets (clusters) of superfluid helium ^{4}He$_N$ [33, 36, 105] that make up a unique isolated reaction medium.

A very interesting and important (in terms of practical applications) temperature dependence of clusters is observed during the formation of nanostructures on the surface and film deposition from clusters [107, 108]. Large clusters ($N \geqslant 10^3$) having a high internal temperature are readily deformed when deposited on a hot surface, giving rise to two-dimensional structures. It was shown in paper [107] by the molecular dynamics method that the YBa$_2$Cu$_3$O$_{7-x}$ clusters with the number of particles $N = 10^3$ and temperature $T_{\text{cl}} \geqslant 2400$ K make up a film of not more than two atomic layers thick during deposition on a pyrolytic graphite surface. Due to high internal energy, hot nanometer-sized clusters are easily deformed on a solid surface from three- to two-dimensional structures. Such transformation of hot clusters occurs even at room temperature of the surface [108]. High energy makes it possible for clusters to easily overcome local potential barriers and reorientate at the surface so as to form a high-quality, uniformly thick film. The technology based on this phenomenon opens up possibilities for growing homogeneous films from high-melting-point superconducting materials [107, 108].

2.3 Temperature of clusters obtained from nozzle sources

The temperature of large clusters generated in nozzle sources can be determined by measuring electron diffraction. An electron beam intersecting a cluster beam forms diffraction rings [109]. Ring diameters give lattice parameters that may be used to estimate lattice temperature from a comparison with the data for bulk matter, taking into account the dimensional effects of the clusters, too. However, such a method is applicable only to clusters undergoing crystallization to the same phase as the bulk matter. In the case of rare gas clusters, it is essential that the cluster should be consisted of roughly 10^3 or more atoms because smaller clusters have a quasicrystalline icosahedral structure instead of a close-packed crystalline structure (see review [43] and references cited therein).

Experiments have shown that the internal temperatures of large clusters from nozzle sources in the absence of a carrier gas are virtually independent of the conditions under which they form, such as gas temperature and pressure in the source. The temperatures of large clusters constitute certain char-

acteristic temperatures of the materials from which the clusters were made. Cluster temperature can be estimated as follows [110, 111]. The atomic lifetime τ on the surface of a cluster with temperature T_{cl} is given by the well-known relation [112]

$$\tau = \tau_0 \exp\left(\frac{\Delta E_s}{k_B T_{cl}}\right), \tag{2.5}$$

where τ_0 is the atomic oscillation period at the surface, ΔE_s is the heat of sublimation or vaporization heat, and k_B is the Boltzmann constant. Cooling of large clusters by evaporation in a high vacuum is completed in a time of order 10^{-3} s if nothing else. This time is commensurate with the time of flight from the source to the electron beam probing the clusters. The dwell time of an atom on the cluster surface ranges about $10^{-2} - 10^{-3}$ s, this time being comparable with or slightly greater than the time of flight [110]. Taking a typical value of 10^{-12} s for the atomic oscillation period τ_0 at the surface, and the value of 10^{-2} s for the atomic lifetime at the cluster surface, one obtains the internal temperature of the cluster as

$$T_{cl} = (10 k_B \ln 10)^{-1} \Delta E_s . \tag{2.6}$$
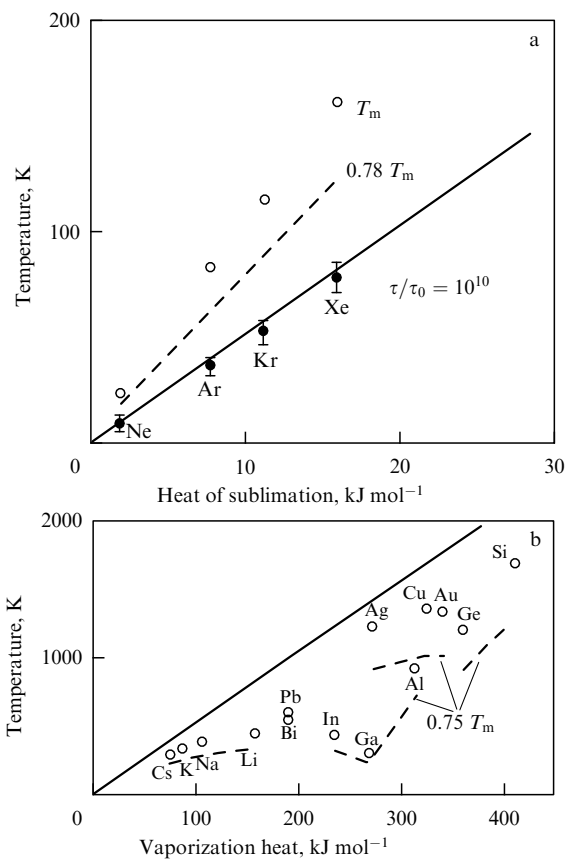
Figure 1. (a) Internal temperatures of clusters formed upon expansion of a pure (without admixtures) gas calculated from relation (2.6) depending on the heat of sublimation (solid line). Experimental data for cluster temperature obtained in Ref. [109] are shown by black circles, melting temperatures T_m of bulk matter by white circles, and low melting temperatures of rare gas clusters with 1000 atoms by the dashed line [110]. (b) Internal temperatures of metallic clusters produced as the pure (without admixtures) vapor expands depending on vaporization heat, calculated from relation (2.6) (solid line). Also shown are melting temperatures of bulk matter (circles) and low melting temperatures of clusters of 1000 atoms (dashed lines) [110].

Figure 1a shows the upper limiting internal temperature of large van der Waals clusters of rare gases as a function of the heat of sublimation for bulk matter [110]. It can be seen that relation (2.6) fairly well describes experimental results. At the same time, the temperature of van der Waals clusters obtained in nozzle sources is not as constant as it may seem from relation (2.6). Cluster temperature depends on the cluster size, which in turn determines the heat of sublimation of the atoms from the cluster surface.

The internal temperature of a free cluster in a vacuum being determined by evaporative cooling (see Sections 2.4 and 2.5), relation (2.6) is applicable to the assessment of the temperature of metal clusters produced by vapor expansion in the absence of a carrier gas (Fig. 1b). Metal clusters obtained by this method are liquid, whereas large clusters of rare gases, produced from nozzle sources without a carrier gas, are solid [43] (see Fig. 1). As shown in Fig. 1a, the temperatures of van der Waals clusters estimated from relation (2.6) are lower than their melting temperatures and therefore even lower than melting temperatures of the respective bulk matter. In contrast, Fig. 1b demonstrates that the temperatures of metallic clusters estimated from relation (2.6) are much higher than the melting temperature of bulk matter and, consequently, even higher than cluster melting temperatures.

2.4 Relationship between cluster temperature and intermolecular interaction potential

There is relationship between cluster temperature and interatomic (intermolecular) interaction potential. The following temperatures of van der Waals clusters were derived by Farges et al. [109] based on crystalline lattice parameters measured using the known values of temperature expansion coefficients [113]: $T_{cl}(Ne) = 10 \pm 4$ K; $T_{cl}(Ar) = 37 \pm 5$ K; $T_{cl}(Kr) = 53 \pm 6$ K, and $T_{cl}(Xe) = 79 \pm 8$ K. It was revealed that cluster temperature grows with strengthening interatomic attraction within the cluster, suggesting that cluster temperature is actually related to intermolecular potential, in agreement with condensation and evaporation processes in cluster beams [114]. As clusters grow in an expanding jet, the heat of condensation is absorbed by the gas, while cluster temperature remains high and constant throughout the period of cluster growth. After the expansion process is completed, the clusters freely move through the vacuum, condensation ceases, but evaporation continues. In other words, cluster temperature decreases until no atom can evaporate. Therefore, the smaller the binding energy between atoms within the cluster, the lower its final temperature.

Assuming the interatomic binding energy in a cluster to be proportional to the depth ε of potential well of the Lennard-Jones potential of an inert gas, it is possible to show (Fig. 2a) that the cluster temperature T_{cl} is proportional to ε. This suggests a constant thermal-to-binding energy ratio for inert gas clusters within a beam.

At the same time, condensation–evaporation processes involving small clusters may result in lower temperatures. It was revealed in Ref. [115] for small amorphous argon clusters ($N < 50$) that $T_{cl} = 27 \pm 3$ K, much smaller than the temperatures of crystalline clusters. The relationship between T_{cl} and ε can be generalized to other clusters. The authors of Ref. [116] used diffraction patterns to estimate temperatures of N_2, O_2, and CO_2 clusters. The results are presented in Fig. 2a along with the data for clusters of inert gases. The
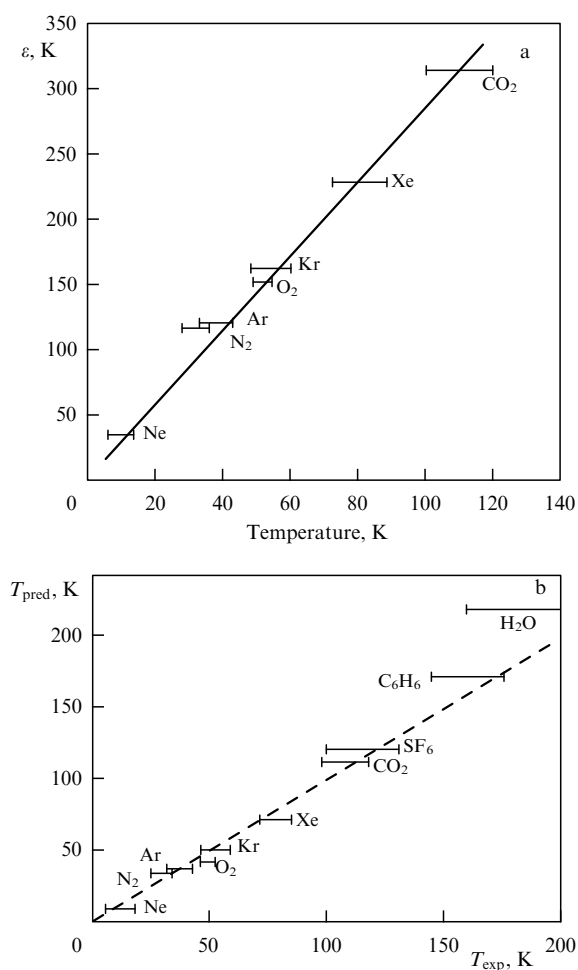
Figure 2. (a) Relationship between the well depth ε of the interatomic or intermolecular potential and estimated cluster temperature in the beam. Experimental results suggest a linear dependence (solid line) [109]. (b) Comparison of measured [124–126] and predicted [from formula (2.8)] (dashed line) temperatures of evaporating clusters [121].

good agreement between these data indicates that the method used to determine argon cluster temperature is also applicable to molecular clusters.

2.5 Relationship between cluster temperature and vaporization heat

The temperature of clusters and nanoparticles can be just as well deduced based on the theory of monomolecular reactions [117, 118]. It is well known that the rates of such reactions strongly depend on temperature. The character of this dependence can be put to use in determining activation energy usually interpreted as a minimal amount of energy localized on the reaction coordinate. In the case of clusters and nanoparticles, dissociation (evaporation) processes are considered using energy instead of temperature for describing a system. Rate constants were exactly computed in the work of Klots [119, 120]. Their principal result that has a direct bearing on the problem of interest in this review consists of the fact that the temperature of an evaporating cluster (aggregate) can be evaluated from the following equation

$$\frac{RT_{cl}}{\Delta E} = \text{const} , \qquad (2.7)$$

where R is the gas constant, and ΔE is the molar vaporization energy. In the rough approximation, the constant on the right-hand side of formula (2.7) is independent of cluster material, being a very slowly decreasing function of time (since the cluster undergoes cooling). On a time scale of a few dozen microseconds, computation gives a typical value of the constant equal to about 4×10^{-2} [120].

Relation (2.7) can also be represented in the form [121]

$$\frac{\Delta}{k_B T_{cl}} \approx \gamma , \qquad (2.8)$$

where Δ is the evaporation (vaporization) energy per particle. Parameter γ, equaling the inverse constant from relationship (2.7), is called the Gspann parameter. As mentioned above, it is virtually independent of cluster size and material but depends only slightly on time and roughly equals 25 on a typical time sale of tens of microseconds. However, detailed analysis recently reported in Ref. [122] indicates that the Gspann parameter may differ from this value by 1.5 times (both upwards and downwards) depending on cluster size, density of states, and kinetic energy realized during cluster evaporation.

Relations (2.7) and (2.8) may be used to predict the temperature of large clusters, e.g., as investigated by the diffraction method. Thermodynamic data entering Eqns (2.7) and (2.8) can be taken from standard sources (e.g., handbook [123]). Figure 2b compares cluster temperatures predicted in Refs [120, 121] and measured in experiments with large van der Waals clusters by the electron diffraction method [124–126]. The dashed line in the figure has a unity slope and is not the best fit to the experimental data. Figure 2b shows that the theoretical prediction is in fairly good agreement with the experiment.

3. Peculiarities of solid–liquid phase transitions in clusters

Before proceeding to experimental methods for determining the cluster melting temperature and the heat of fusion, let us consider certain results of theoretical research and computer simulation of solid–liquid phase transitions in clusters to obtain a deeper insight into this process and to seize the essence of the problems reviewed.

The solid–liquid phase transition in clusters is described in the framework of classical thermodynamics and is more complicated than in bulk matter [7, 25, 38]. The statistical model developed to describe clusters facilitates understanding the aggregate state from the microscopic standpoint. The most noticeable progress in addressing this issue has been achieved in investigations of phase transition in clusters by computer simulation. The cluster as a system of a finite number of bound atoms is better suited for computer analysis than a macroscopic system. Moreover, phase transition is a collective phenomenon involving many atoms. Numerical computer-assisted methods allow this fact to be taken into account, unlike analytical methods using a one-particle approximation. Also worthy of note is that clusters are a convenient model for describing macroscopic systems. In what follows, we shall briefly discuss at the qualitative level certain results of phase transition studies in clusters. This problem is expounded at greater length in the work of R S Berry's group [65, 127–139], D J Wales [64, 65, 140–146], and B M Smirnov [7, 38, 59, 60, 147, 148] (see, for example, reviews [7, 25, 38, 45] and references cited therein).

The most important results of solid–liquid phase transition research in clusters and nanoparticles can be summarized as follows: (1) the coexistence of two phases within a certain temperature range in the vicinity of thermodynamic equilibrium temperature; (2) the representation of the solid–liquid phase transition as configuration excitation, and (3) the possibility of the occurrence of negative heat capacity of a cluster near the melting point.

3.1 Coexistence of two phases
An important distinctive feature of solid–liquid phase transition in clusters compared with the analogous transition in macroscopic systems is the coexistence of liquid and solid states within a certain temperature range in the vicinity of the melting point [7, 38, 128–140, 148, 149]. Theoretical research and computer simulation studies conducted even in the 1970s demonstrated [150–154] that clusters of atoms and molecules may exhibit two (or more) stable states corresponding to liquid and solid forms. Under appropriate conditions, these states may just as well correspond to other forms, for example, glassy-like [38, 147] or slush-like [59, 129, 137–139]. We shall consider here the coexistence of solid and liquid states. Coexistence of these phases means that for a particular period of time, a cluster is in the solid state, and for another period of time, it is a liquid.

The essence of the two-phase coexistence phenomenon is as follows. A cluster (particle) containing a finite number of atoms N in thermal equilibrium has a distinct temperature region bounded from below by the temperature T^*_{sol} of transition to the solid state, and from above by the temperature T^*_{liq} of transition to the liquid state. Within this region, the cluster stays in either solid or liquid form. Only the liquid form is stable for a temperature $T > T^*_{liq}$, and only the solid one for $T < T^*_{sol}$. These two temperatures are not equal for a finite number of particles, at least for small N. The temperature difference is the region of coexistence of the two phases, $\Delta T_{co} = T^*_{liq} - T^*_{sol}$; it tends to zero as $N \to \infty$. Such a property is not inherent in each type of clusters. For example, it is lacking in clusters formed from ^{4}He atoms.

There is a temperature $T_{eq}(N)$ within the said coexistence region for which free energies of the solid $[F_{sol}(N, T)]$ and liquid $[F_{liq}(N, T)]$ states are equal [38, 60, 131, 136, 149]. This temperature, i.e., thermodynamic equilibrium temperature, can be called the cluster melting temperature. The phenomenon of coexistence of the two phases is underlain by the fact that the microcanonical dependence (or curve) $T(E)$ can contain a van der Waals 'loop' or 'S-shaped kink' (see Section 3.3). The presence of such a loop in the $T(E)$ dependence suggests the existence of a temperature range in which two stable states of the system are possible, the energy distribution function being bimodal [65, 128, 139]. Such S-shaped kinks in the $T(E)$ curve were found in calculations based, for example, on the density of states at constant pressure and volume [62–67].

It is worth noting that the coexistence of two phases in clusters should not be understood in the statistical physical sense under conditions when all parameters of the system are averaged over a long period of time sufficient for them to come into equilibrium. The phase coexistence is possible only in the dynamic sense under conditions when thermodynamic quantities, such as kinetic energy and entropy, are averaged over a short time period (see also Section 3.3). Only in this case can two (or more) different phases corresponding to the solid or liquid states coexist in a cluster [128–133]. Different
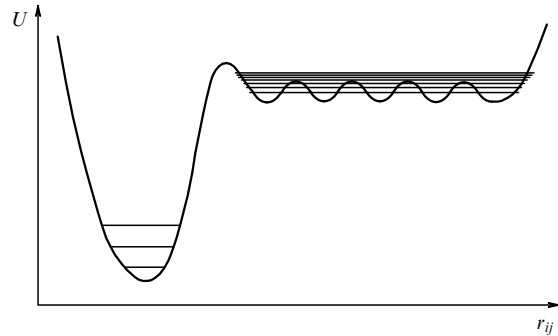
Figure 3. Schematic of a system having a deep and narrow potential well with a rarefied level structure corresponding to the solid phase, and a broad high-energy region with shallow potential energy minima and high density of states corresponding to the liquid phase. The two regions are separated by a potential barrier that ensures the independent existence of either form [131].

phases can be related to different areas of the cluster potential energy surface (PES) (Fig. 3). In other words, dynamic coexistence of two phases in clusters is analogous to fluctuations between two geometric structures (isomers) of a molecule that must have their own characteristic temperatures in the microcanonical ensemble.

3.2 Configuration excitation of clusters
Formation of a liquid aggregate state is mediated through configuration excitation that in the case of a macroscopic system consists in the formation of voids and vacancies inside it [7, 25, 38]. Configuration excitation of a system may be considered in terms of its electron energy. However, it is more frequently considered regardless of a change in the system's electronic state, i.e., when atoms travel over a single electron energy surface or an electronic landscape (as it is termed when applied to clusters) [7, 38].

The evolution of simple clusters composed of inert gas atoms is usually regarded as classical atomic motion in potential wells created by atom–atom interactions. This approach was initially employed in computer-aided calculations [155, 156] of cluster energy. If the aim is to determine the minimal internal energy of a cluster and the corresponding internal configuration of the constituent atoms, one may start from an arbitrary configuration and calculate the energy for it. Thereafter, the atoms need to be displaced, so that the new configuration results in a lower cluster energy. This approach might be hoped to yield a global minimum for the cluster energy and the corresponding optimal configuration of the atoms in the cluster. However, such a program cannot be realized because the cluster potential energy surface has many local minima and saddle points. For example, a cluster with the Lennard-Jones interatomic interaction potential (or Lennard-Jones cluster) consisting of 13 atoms has 988 local minima of the PES [155, 156]. A more detailed analysis [157] revealed 1478 local minima and 17,357 saddle points for the PES of this cluster. The number of local minima increases exponentially with the number of atoms in the cluster [158, 159]. Adjacent local minima at cluster multidimensional PESs are separated by potential barriers characterized by saddle points [25, 38, 59, 60].

With these PES properties in mind, the evolution of clusters in time is regarded as a series of transitions between the neighboring local minima of multidimensional PES space

[136, 143, 144, 160, 161]. Analysis of the saddle-crossing dynamics [162] is a tool for studying cluster evolution. Potential barriers account for the cluster dwell time near a given PES minimum [163] to be rather long compared with the characteristic atomic oscillation time in the cluster ($\approx 10^{-12} - 10^{-14}$ s). As a consequence, the separation of thermal and configuration excitation energies of a cluster takes place. The former is determined by the thermal energy of atomic oscillations and rotations, while the latter is characterized by a given local PES minimum [38, 60]. At zero temperature, only the configuration part of the energy (responsible for cluster excitation with respect to the global PES minimum) is retained, whereas at high temperatures, the kinetic energy of atomic motion is considerably higher than the configuration excitation energy [43].

The possibility of breaking up the cluster energy into configuration and thermal components allows for the analysis of the atomic dynamics inside the cluster [25, 38, 60]. In the framework of this approach, the nature of phase transition can be described in terms of the lattice model [164–167] according to which the cluster atoms occupy lattice sites. This model can be simplified by taking into account only nearest-neighbor interactions. In this model, for example, in the case of a square crystalline lattice, two limiting distributions of atoms are considered [38, 167], viz. compact or ordered distribution with a maximum inter-atomic binding energy, and chaotic or disordered distribution. The latter is characterized by a lower binding energy compared with the former one but, however, is much more realizable, i.e., its statistical weight and, accordingly, entropy are large numbers. It accounts for the possibility of order–disorder phase transition in such a system. If the system contains a large number of atoms, its phase transition proceeds through a stepwise change of internal energy and entropy at a given temperature at which the free energies for the atomic distributions being considered become equal. Thus, the lattice model sheds light on the nature of the first-order phase transition in systems with a large number of bound atoms. The order–disorder phase transition simulates the solid–liquid phase transition for real systems and depends on configuration excitation of the atomic ensemble.

In the framework of the lattice model, the void or the vacant site is considered to be an elementary configuration excitation of a system [168]. The void is regarded as an excited vacancy but its volume and shape vary with time unlike a vacancy in a solid. In the context of saddle point dynamics, each configurationally excited state corresponds to the formation of a certain number of voids in the system. The concept of voids with averaged parameters is valid when configuration excitation is separated from the thermal one related to oscillatory atomic motion. In this case, the liquid aggregate state of a cluster is defined as the totality of its configuration states with closely related excitation energies (see Fig. 3), i.e., with energies near the corresponding local PES minima of the cluster in the multidimensional space of atomic coordinates [38, 148].

The above definition of the aggregate state differs from the one accepted in classical thermodynamics, where the phase is interpreted as a uniform spatial distribution of atoms. Therefore, such an excited aggregate state in the case under consideration must contain many elementary configuration excitations. However, the liquid aggregate state of a cluster may have only one elementary excitation, which makes the condition of uniform spatial distribution unnecessary. For example, phase transition to the liquid state for a cluster consisting of 13 atoms and having an icosahedral structure occurs upon the passage of a single atom from the filled shell to its surface [7, 25, 38]. Formation of the liquid aggregate state in large clusters is associated with the development of many voids. In the framework of the void concept, the coexistence of liquid and solid phases in a cluster is a result of void formation and destruction [38, 60].

A detailed description of cluster evolution implies new criteria for cluster melting and leads to a discrepancy with classical thermodynamics where the Lindemann criterion is used as a melting criterion [169, 170], according to which the ratio of atomic oscillation amplitude to mean interatomic distance at the melting point reaches a definite value (ca. 10–15%). More accurate melting criteria became available with the development of numerical computer simulation techniques, e.g. the Etters–Kaelberer criterion [152–154] and the Berry criterion [149, 171] based on the correlation between pair distribution functions of atoms in space. The corresponding parameters change in a stepwise fashion and reflect variations of thermal atomic motion during melting, as in the case of the Lindemann criterion, while the nature of the phase transition relates to configuration excitation of a cluster. This suggests a discrepancy between the nature of phase transition and practical criteria for its analysis. However, the results of investigations show that thermal atomic motion makes an important contribution to the entropy jump ΔS during phase transition [25, 38]. This justifies the application of practical melting criteria based on thermal atomic motion.

Thus, consideration of the liquid aggregate state as a configurationally excited state of an ensemble of bound atoms that is, in turn, associated with void formation inside the system makes it possible to analyze the solid–liquid phase transition in clusters and to study different properties and processes in such ensembles [25, 38, 59, 60].
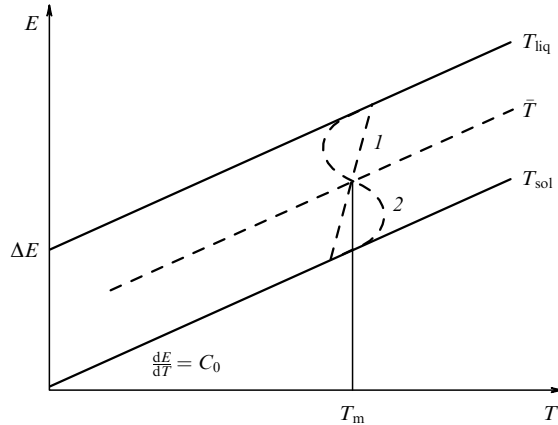
3.3 Negative heat capacity of a cluster near the melting point

Another distinctive property of clusters versus bulk matter (besides the coexistence of two phases) is the possibility of observing negative heat capacity near the melting point. The negative heat capacity of a cluster was first predicted in Refs [62, 63] and examined experimentally in Ref. [70] by the example of Na_{147}^{+} cluster ions. References [38, 60, 62–67] also predict negative heat capacity of clusters near the melting point, and Refs [70–73] report its observation in experiment. Let us briefly consider the possibility of existence of cluster negative heat capacity in the framework of two-aggregate-state approximation [38, 59, 60].

The heat capacity of a cluster is defined by the relation

$$C = \frac{dE}{dT}, \tag{3.1}$$

where the variation dE refers to the total cluster energy which includes oscillatory atomic motion and configuration excitation, while translational temperature T characterizes thermal atomic motion alone. To recall, the relationship between temperature and energy, $E = E(T)$, is referred to as the caloric curve. In the framework of the approximation of two aggregate states and on the assumption that the cluster caloric curves are straight parallel lines (Fig. 4), we have the following expression for the variation of cluster translational

Figure 4. Caloric curves of an isolated cluster with two aggregate states in the one-temperature approximation [60]: *1* — the case of positive heat capacity, and *2* — the case of negative heat capacity of the cluster near the melting point.

temperature [38, 60]:

$$dT = dT_{sol} - \Delta T \, dw_{liq} \,, \qquad (3.2)$$

where dT_{sol} is the variation of translational temperature of solid-phase cluster atoms, ΔT is the temperature difference between solid and liquid phases, and w_{liq} is the probability of finding cluster in the liquid state, which is related to the probability w_{sol} of finding cluster in the solid state by the normalization equation

$$w_{sol} + w_{liq} = 1 \,. \qquad (3.3)$$

On the other hand, the temperature of a cluster with two aggregate states in the region of coexistence of two phases can be represented [38, 60] as

$$T = w_{sol} T_{sol} + w_{liq} T_{liq} \,, \qquad (3.4)$$

where T_{liq} is the temperature of the liquid phase. Let us introduce the energy of cluster thermal excitation

$$dE_{th} = C_0 \, dT_{sol} = C_0 \, dT_{liq} \qquad (3.5)$$

responsible for the cluster motion along one of the parallel caloric straight lines (Fig. 4), where C_0 is the cluster heat capacity far from the melting point [38, 60], and the configuration excitation energy

$$dE_{con} = \Delta E \, dw_{liq} \qquad (3.6)$$

responsible for the movement between these lines. Then, for the total energy change dE of an isolated cluster [38, 60], we have

$$dE = dE_{th} + dE_{con} = C_0 \, dT_{sol} + \Delta E \, dw_{liq} \,. \qquad (3.7)$$

Under the conditions being considered, equilibrium is reached at each new energy of the cluster, and each small rise in the energy near the melting temperature is partly spent to excite the thermal atomic motion and partly to maintain configuration excitation. If a new small portion of the energy transferred to the cluster induces configuration excitation and passes to the configuration degree of freedom (as a small

fraction of thermal atomic energy does), the effective cluster temperature defined as the mean kinetic energy per degree of freedom decreases with increasing cluster energy. This case is known as the *S*-shaped kink in the caloric curve (Fig. 4). Such behavior of the cluster ensues from both theoretical analysis [62–67] and experimental results [68–73].

Assuming that an isolated cluster is characterized by two temperatures, translational and configurational, and using relations (3.2) and (3.7) for the variations of translational temperature T and total cluster energy E, the heat capacity of the isolated cluster can be expressed as [38]

$$C = \frac{dE}{dT} = C_0 \frac{1 + x}{1 - x} \,, \quad x = \Delta T \frac{dw_{liq}}{dT_{sol}} \,. \qquad (3.8)$$

In deriving formula (3.8), we took into account that under the given conditions $\Delta E = C_0 \Delta T$. Hence it follows that the heat capacity of an isolated cluster is negative near the melting point, where condition $x > 1$ is fulfilled for the parameter x [38, 60].

It should be noted, however, that it is incorrect to state the problem of the heat capacity of an isolated cluster, for at least two reasons [38]. First, a cluster with two aggregate states is described by two different translational temperatures. Therefore, consideration of cluster heat capacity, a thermodynamic quantity, in the conditions of a departure from thermodynamic equilibrium is not quite correct. Second, configuration excitation temperature does not coincide with the cluster translational temperature, meaning that the procedure of bringing a cluster into a thermodynamically equilibrated state described by one temperature rather than two, as in the above analysis, is not strict enough. Therefore, although the negative slope of the caloric curve is feasible it does not meet strict thermodynamic conditions [38] (see also Section 3.1). Thus, it is possible to obtain a negative heat capacity of an isolated cluster at or close to the melting temperature, but it will not correspond to the thermodynamic equilibrium at which the heat capacity is defined [38, 60].

4. Methods for measuring the melting temperature and the heat of fusion of clusters

4.1. General remarks. Dependence of melting temperature on cluster size and structure

Macroscopic matter has a well-defined melting temperature T_m at a given pressure. Melting of matter becomes apparent as a change in the specimen shape and can be visually observed. In contrast, clusters have no fixed melting temperature (see Section 3.1). Their solid and liquid phases coexist in a certain temperature region. A variety of properties manifest themselves in clusters during their melting. Measurement of the melting temperature and heat of fusion of clusters encounters difficulties. For particles with $N = 10^3 - 10^6$ atoms, diffraction methods are suitable (see, for instance, review [43] and references cited therein). However, the difficulties in measuring the cluster melting temperature grow further as the size of the particles decreases. At the same time, melting temperature is one of the major physical characteristics of clusters and is especially important in the context of their theoretical and practical applications because it determines the damage threshold of nanostructural elements, systems, and thin films.

Small particles have a lower melting temperature than corresponding bulk matter. This peculiarity was first pre-

dicted theoretically in Ref. [172] and later confirmed experimentally in Ref. [173]. The physical cause of this phenomenon can be explained in qualitative terms using the Lindemann criterion [169, 170] as follows. The surface atom fraction of small particles is much greater than in macroscopic bodies. Surface atoms have fewer neighbors; therefore, they are loosely bound and their thermal motion is less restricted than in bulk matter [174]. However, as mentioned in Section 3.2, there are other more accurate cluster melting criteria based on pair correlation functions for spatial atomic distribution [152, 153].

Cluster melting has been investigated in many studies, both experimental [68 – 73, 175 – 186] and theoretical [62 – 67, 127 – 149, 187 – 198]. There are three main differences between solid–liquid phase transitions in clusters (systems of limited size) and macroscopic bodies: (1) melting temperature drops with decreasing particle size; (2) phase transition occurs within a limited temperature range, and (3) the particles' heat of fusion is lower than that of macroscopic matter. It has also been found that the melting temperature of small clusters ($N \leqslant 200$) undergoes marked fluctuations, depending on their size [69, 71, 176] (Fig. 5), due to the relationship between cluster structure and its size, and the existence of magic numbers. The heat of fusion of certain clusters may exceed that of bulk matter, which suggests their extraordinarily robust structure [199 – 202]. Phase transition may be accompanied by the initial melting of cluster surface layers [190, 197, 203], the sequential melting of various cluster shells [203, 204], and orientational melting [205, 206]. Calculated results show that the replacement of a single cluster atom with an impurity atom in metallic clusters ($N = 55$) may significantly increase [207] or decrease [208] (see also Ref. [209]) their melting temperature due to a sharp change in the electronic and/or atomic shell structure of the cluster. The melting temperatures of clusters resided on a substrate is in the general case higher than that of free ones [210] because they give up their energy to the surface. Moreover, interaction with the substrate may lead to marked changes in cluster shape and structure [211, 212], and hence to a change in melting temperature. This considerably complicates interpretation of substrate influence on cluster melting temperature [211]. Both melting temperature and the heat of fusion decrease approximately linearly with decreasing cluster radius [203, 213, 214]. There is a correlation between cluster temperature and heat of fusion and the atomic binding energy in a cluster: the greater the latter, the higher the temperature and heat of fusion [215]. Thin oxide film-coated clusters possess a higher melting temperature due to enhanced surface tension force [216]. Both experiments [70 – 73] and calculations [62 – 67] also indicate that clusters may have negative heat capacity near the phase transition point (see Section 3.3). The nature of this phenomenon arises from the fact that energy in such complicated systems is not an extensive quantity. Of great importance is the interaction between cluster subsystems that cannot be neglected [38, 190, 194].

## 4.2 Early methods for measuring the melting temperature of clusters

The first measurements of cluster melting temperature with a transmission electron microscope were made by Takagi [173]. The method was based on a change in the diffraction pattern at the melting point due to disordering the cluster structure. The melting temperature decreased with decreasing cluster
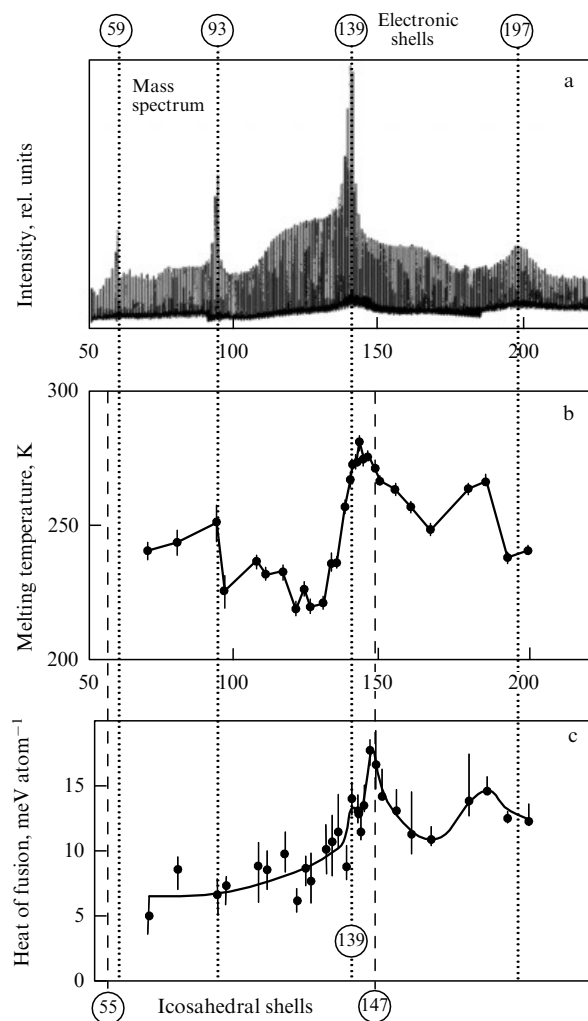
Figure 5. Three different sets of data represented with reference to cluster size. (a) Mass spectrum of hot positively charged sodium clusters ($T \approx 400$ K). Enhanced intensities of mass peaks in 'magic' clusters are attributable to higher dissociation energies for clusters with completely filled electronic shells (top). Numbers (59, 93...) correspond to the number of atoms in a cluster. (b) Cluster melting temperatures. The values vary considerably depending on cluster size and weakly correlate with the filling of electronic shells. Melting temperature of bulk sodium (371 K) is much higher than that of clusters. (c) Cluster heat of fusion. For bulk matter it equals 27 meV per atom. The number of atoms at which filling of icosahedral shells occurs is shown at the bottom [69].

size. It should be noted, however, that the electron diffraction method is unfit for studying small clusters due to the low intensity of diffraction lines and their broadening (see review [43] and references cited therein). Moreover, it being sensitive to cluster structure alone, heat of fusion has to be measured by a different technique.

Melting temperature of lead clusters with a radius of 100 – 500 Å was determined in Ref. [177] by measuring reflective power R of particles inserted into a transparent matrix. The reflectivity of this material is different in the liquid and solid phases; therefore, measuring its temperature dependence can be used to determine phase transition temperature. A jump in $R(T)$ dependence with increasing temperature has been documented for clusters of different sizes in a range from 390 to 460 K (Fig. 6). Analysis of these measurement data [177] revealed that melting temperature falls as the particle size decreases. It should be emphasized,
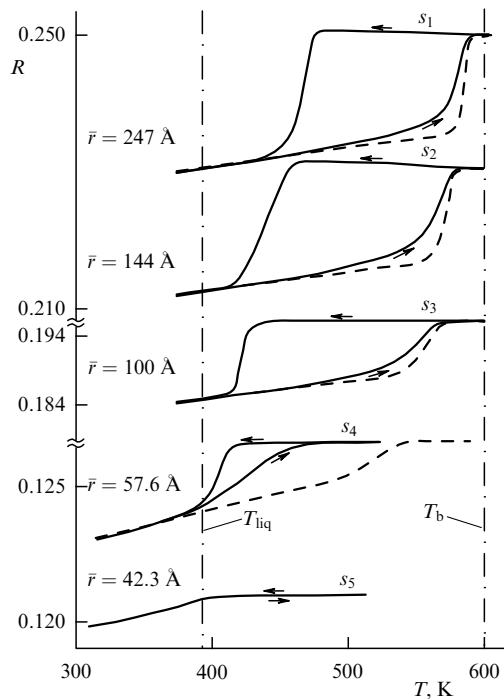
Figure 6. Reflection curves for five different distributions of lead nanoparticles by size ($\bar{r}$ — mean cluster radius in a given distribution, $s_1 - s_5$ — sample numbers). Solid lines are experimental results. $T_{liq} \sim 392$ K is the maximum temperature of fluid overcooling. Dashed lines are theoretical results. T_b is the melting temperature of bulk lead [177].


Figure 7. (a) Size dependence of the melting temperature of tin clusters. (b) Size dependence of normalized heat of cluster fusion. Dots are experimental data, and the solid line presents calculated values [178].

however, that their results could be influenced by surface melting of the clusters.

The calorimetric technique for measuring melting temperature of large clusters has been developed by Lai et al. [178], who studied melting of tin particles with a radius of 50 – 500 Å containing up to 10^7 atoms. The particles were deposited onto the surface of an SiN thin-film calorimeter. The measurements were performed by feeding an electric pulse to a heater consisting of a thin Ni film. The pulse heated the system incorporating the heater, SiN membrane, and an Sn sample. The authors measured in real time the current passing through the system and the applied voltage. The energy consumption rate increased as soon as the tin particles began to melt. Analysis of changes in heater resistance with time yielded exact values of system temperature and total energy deposited into the system. It was found that the melting temperature of the clusters drops sharply (from roughly 220 to 150 °C) as their average radius decreases from 500 to 50 Å (Fig. 7). For bulk matter, $T_m = 232$ °C. The heat of cluster fusion also markedly decreased from 58.9 J g^{-1} (for bulk matter) to ≈ 16 J g^{-1}, i.e., by approximately 70%.

The solid–liquid phase transition can be identified from the cluster fragmentation pattern [175, 179]. If clusters undergoing dissociation are in the liquid phase, the magic numbers will not be seen in their fragmentation structure because cluster stability is a function of structure and a liquid has no ordered structure whatever. Conversely, if the magic numbers are well apparent in the fragmentation structure, it suggests a solid structure of the cluster undergoing fragmentation. Dissociation of a solid particle is regarded here as an analog of sublimation.
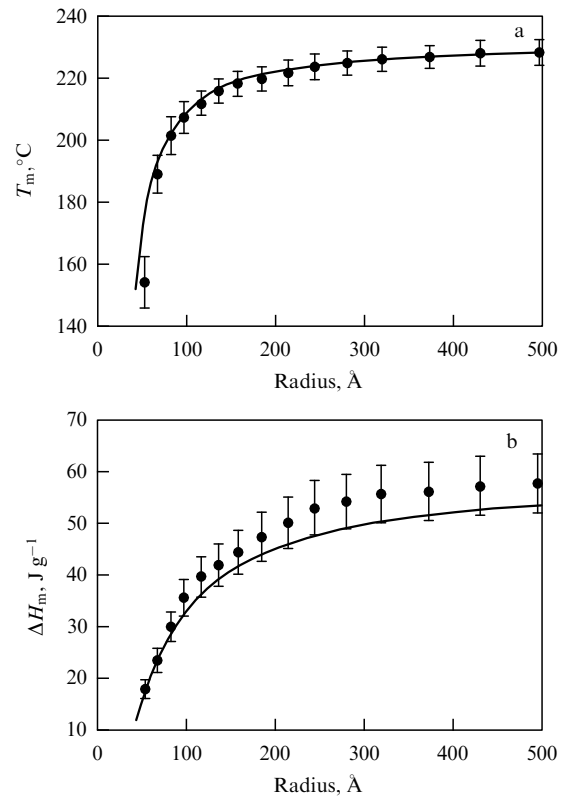
4.3 Optical methods for measuring the melting temperature of clusters

The melting of clusters was also deduced in Refs [180, 181] from changes in the spectral characteristics of free composite clusters, such as an inert gas cluster with a large molecule inserted into it. The temperature dependence of cluster optical properties [217 – 226] is attributable to two causes — a structural change, and a change in the phase state. Thus, the evaluation of absorption cross sections of sodium Na_8 clusters by the Monte Carlo method [217] showed that their equilibrium structure has symmetry group D_{2d}. The photoabsorption cross section for such a geometry is characterized by two peaks, whose energies are separated by 200 meV (Fig. 8a). It was revealed that the absorption cross section strongly depends on the cluster vibrational temperature. The two-peak structure persists to a temperature of roughly 100 K. It changes above this value, with a gradual opening of a new phase space. At a temperature above the melting point, the two-peak spectrum transforms into a spectrum with one broad asymmetric peak that fairly well reproduces experimental results obtained at the same temperature (Fig. 8b).
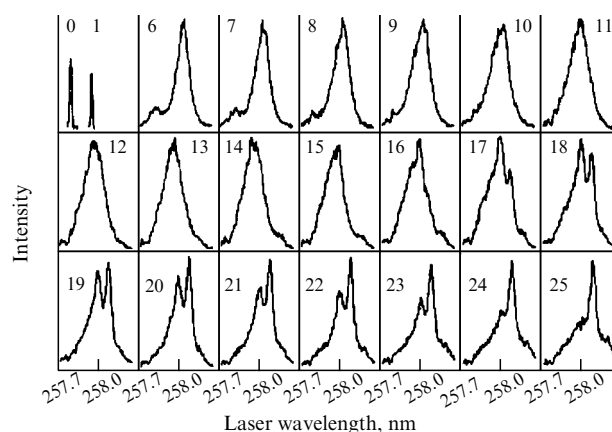
The strong temperature dependence of photoabsorption cross sections was also observed for Na_N^+ cluster ions in Refs [218] ($N = 4, 7, 11$) and [219] ($N = 9, 21, 41$). Thus, Ref. [218] reported six separate absorption lines for cold Na_{11}^+ cluster ions ($T \sim 35$ K). These lines were interpreted as separate transitions between electronic states of the Na_{11}^+ molecule. At a high temperature ($T > 380$ K), when the clusters become liquid, the spectrum exhibits two broad peaks. Their energetic position for clusters with $N > 7$ is fairly well described by a model in which almost free electrons oscillate in a spherical container. Single wide absorption
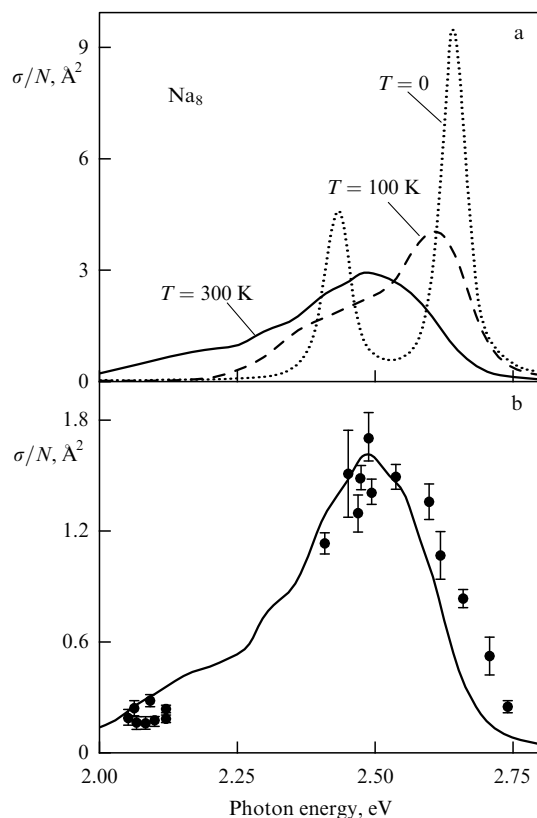
Figure 8. Calculated photoabsorption cross sections of Na_8 clusters (a) at three different vibrational temperatures, and (b) at $T = 300$ K: theoretical curve and experimental data (dots) obtained at 300 K in Ref. [226]; the theoretical curve (solid line) is normalized to bring all calculated values into agreement with experimental findings (taken from Ref. [217]).

Figure 9. Optical absorption spectra of argon clusters doped with C_6D_6 molecules (C_6D_6/Ar_N, $N = 0-25$) in the transition region 6_0^1 of a benzene molecule. The spectra were obtained with a photoionization time-of-flight mass spectrometer. The clusters were generated in a gas-dynamic jet as the Ar:He (15:85) mixture expanded at a total gas pressure of 9 atm above the nozzle [220].

peaks were observed in Ref. [219] at a high cluster temperature ($T > 300$ K), and much narrower ones at 130 K. In the case of Na_9^+, two absorption peaks spaced 275 meV apart were observed at low temperatures. It should be noted, however, that it is impossible to determine the melting temperature of clusters from the temperature-dependent evolution of absorption spectra [227].

The solid–liquid phase transition can be identified from optical absorption spectra [220] in argon clusters doped with benzene molecules C_6D_6. Using the second harmonic of a dye laser and single-frequency two-photon resonance ionization of C_6D_6 in argon clusters, the authors of Ref. [220] demonstrated that clusters in solid and liquid phases coexist in a beam within a certain temperature region, as evidenced by the presence of two lines of different shapes corresponding to absorption by solid and liquid phases in the electron absorption spectrum of C_6D_6 molecules within the range of $257.7-258.0$ nm. Figure 9 shows that the absorption spectrum of argon clusters with $N = 6-15$ is a wide (ca. 30 cm^{-1}) structureless band, whereas a well-apparent structure is clearly seen against the background of the broad band of bigger clusters (from $N = 16$). Such a shape of the spectra can be accounted for by the coexistence of solid and liquid phases of the clusters [220]. It is possible to determine the fraction of either phase from the integral intensity of the absorption lines. Experiments of this type directly confirm the theoretical predictions (based on quantum-statistical consideration of cluster properties) of two different temperatures for clusters (in contrast to macroscopic substances),

namely melting temperature and crystallization temperature, separated by a well-defined coexistence region of two phases [38, 129, 130, 187].

Similar results were obtained in Ref. [228], where the laser double-frequency two-photon resonance ionization technique was utilized to study absorption spectra of mass-selected free heteroclusters of dichloranthracene with krypton (DCA/Kr$_N$, $N = 1-20$) in a molecular beam. The vibrational temperature of DCA molecules determined from 'hot' band intensities in clusters with $N = 1-3$ ranged $T_v = 20-30$ K. Cluster structure and phase transitions were deduced from the shape, width, and pattern of absorption spectra of the DCA molecule at the $S_0 \rightarrow S_1$ transition and from the spectral red shift, depending on the number of krypton atoms in the cluster [228]. Figure 10 shows structureless and rather wide (from 25 to 70 cm^{-1}) absorption spectra of clusters with $N = 10-16$, the width of which grows with increasing N. A sharp change from a structureless to a structured spectrum and a decrease of its width occur at $N = 17$ due to alteration of the cluster structure (transition from liquid to solid state) [228]. Thus, papers [220, 228] provide spectroscopic evidence of phase transitions in heteroclusters. Notice that these transitions are associated with changes in cluster size at practically constant temperature, whereas the temperature of solid–liquid phase transition in clusters grows with increasing N.

Temperature-related variations of absorption spectra caused by structural changes in the clusters may be used to determine the temperature of structural transitions. Comparison of experimental and *ab initio* calculated spectra of vibrational predissociation of protonated methanol clusters $H^+(CH_3OH)_4$ and $H^+(CH_3OH)_5$ in Ref. [222] yielded a temperature of cluster transition from one isomeric configuration to another ($T_{cl} = 190$ K). Similar structural changes were observed in vibrational predissociation spectra of protonated water clusters $H^+(H_2O)_{5-8}$ [224].

4.4 Calorimetric methods for measuring the cluster melting temperature and heat of fusion in a molecular beam
This section is designed to consider the calorimetric method for measuring the temperature and heat of fusion of clusters
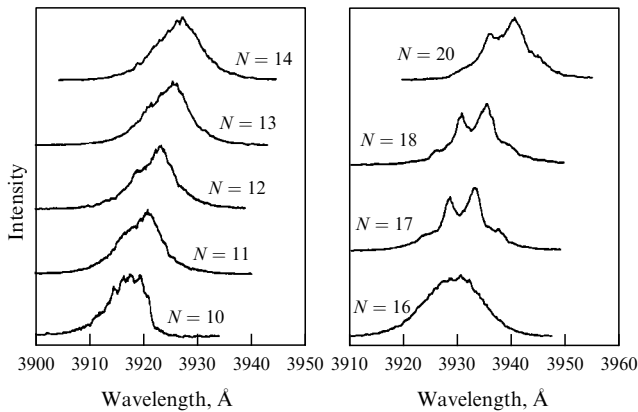
Figure 10. Optical absorption spectra of mass-selected DCA/Kr$_N$ clusters ($N = 10-20$) in a pulsed supersonic jet (30% He and 70% Ne). The spectra were obtained by double-frequency two-photon resonance ionization using a time-of-flight mass spectrometer [228].

in a molecular beam, which was developed in Ref. [186]. Experiments were done with free tin clusters (mean size $\overline{N} \sim 500$) distributed in size in a molecular beam, unlike the experiments described in Ref. [178] (see Section 4.2) where the melting temperature of large tin clusters attached to a substrate was measured by the calorimetric method. In other words, the influence of the substrate on melting temperature was totally excluded in Ref. [186]. Moreover, the use of molecular beams made it possible to study the temperature behavior of small clusters.

The experimental setup with a calorimeter is displayed in Fig. 11 [229]. The cluster beam was incident on a thin Mo(100) or W(100) single crystal (1 µm thick, 10 mm in diameter) enclosed between two tantalum (Ta) plates 0.25 mm in thickness, each having a central hole 7 mm in diameter. Using a manipulator, the single crystal with a holder could

be placed in the socket of the massive thermoregulator. The calorimeter-attached pyroelectric detector had a sensitive element based on the pyroactive foil 4×20 mm in area and 9 µm in thickness representing a dense sticky β-polyvinylidene (PVDF) ribbon covered with 20–60-nm thick gold or NiAl contact electrodes on both sides. Such film is usually used in IR detectors. The arched shape of the detector's strip ensured its close contact with the single crystal during displacements of the detector (Fig. 11). The contact area for a pyroelectric ribbon and a single crystal amounted to about 16 mm^2. Measurements were based on the fact that the heat brought in by clusters to the single-crystal surface was further transferred to the pyroelement (for ~ 1 s) and induced an electrical signal that was amplified 100 times at the detector output. The sensitivity of the detector was roughly 10 V J^{-1} and incidentally amounted to 100 V J^{-1}, furnishing reliable detection of cluster beam-induced heat on the single crystal.

The authors of Ref. [186] determined the energy of cluster formation in the molecular beam depending on gas temperature above the nozzle. To this end, they measured (with the above-described nanocalorimeter [229]) the heat released during condensation of tin clusters from the incident molecular beam onto the solid tin surface on the single crystal. The results were used to estimate the energy of generation of free clusters.

Internal cluster temperature varied as a result of changes in the nozzle temperature. It was assumed [186] that the carrier gas (helium) and the arising tin clusters are in thermal equilibrium at the nozzle temperature. Such an assumption is quite admissible, bearing in mind rather high nozzle temperature ($\geqslant 300$ K) and low gas pressure above the nozzle in the given experiment, where adiabatic expansion of the gas into the vacuum could be neglected. Due to this, the internal (vibrational) temperature of the clusters was only slightly (by $10-20$ K at most) different from the nozzle temperature. The experimental results cited below show that this circumstance may be used to control internal cluster temperature.
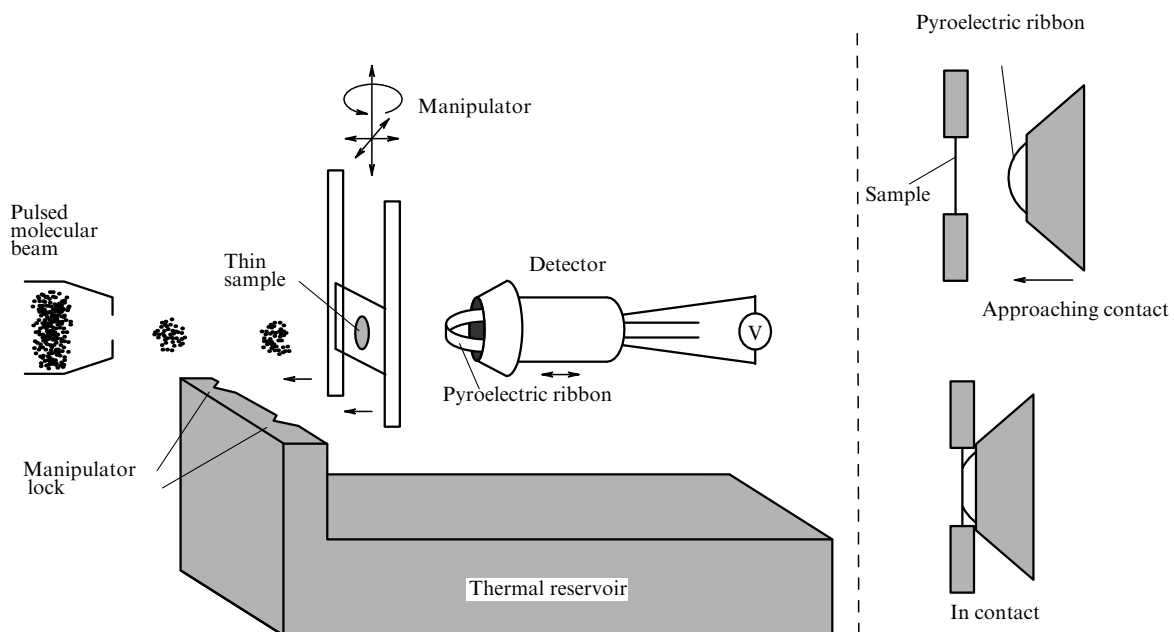
Figure 11. Diagram of a high-vacuum calorimeter with a movable detector based on a thin pyroelectric film. Enlarged drawing on the right side shows the detector approaching the sample and in contact with it [229].
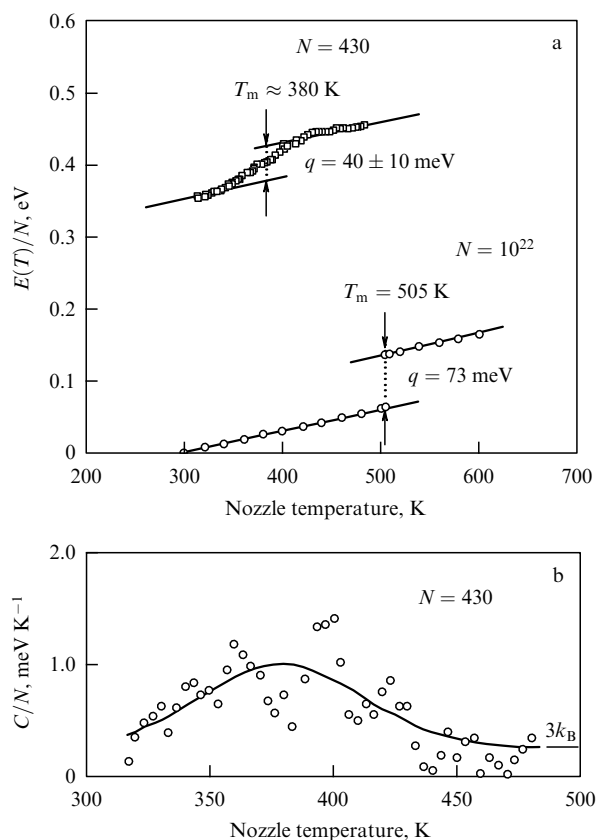
Figure 12. (a) Temperature dependence of internal energy per atom $E(T)/N$ for isolated tin clusters (squares) and bulk tin (circles). (b) Heat capacity $C(T)/N$ of isolated tin clusters with a mean size $\overline{N} = 430$. Solid lines in both figures are drawn for a better view of the data [186].

Figure 12a illustrates the temperature dependences of the internal energy of tin clusters (mean size $\overline{N} = 430$) and bulk tin [230] for which the internal energy at 298 K is assumed to equal zero. The temperature dependence of the internal energy of tin clusters gives convincing evidence of a greater rise in energy within the temperature range from 340 to 420 K compared with two other regions, below 340 K and above 420 K. In these regions, the cluster internal energy undergoes a linear increase as temperature rises, with a slope of approximately $3k_B$ (k_B is the Boltzmann constant), in agreement with the Dulong–Petit law. Such behavior of this dependence in the 340–420 K range can be interpreted as a solid–liquid phase transition in isolated tin clusters. It was shown that the melting temperature of the clusters is roughly 125 K lower than that of the bulk matter, and the latent heat of fusion q reaches 40 ± 10 meV per atom versus 73 meV per atom for bulk matter [230]. In another experiment [186], the authors studied the temperature-dependent behavior of bigger clusters with a size distribution centered around the average value of $\overline{N} = 520$. A similar value of the cluster melting temperature was obtained, while the latent heat of fusion reached 54 ± 10 meV per atom.

Figure 12b depicts the temperature dependence of the latent heat of fusion for tin clusters. It can be seen that phase transition occurs in a temperature region approximately 80 K in width. The broad temperature range of phase transition can be attributed not only to the rather wide size distribution of clusters (the beam contained clusters with N approximately ranging between 100 and

900) but also to the presence of the temperature region with two coexisting phases [69, 186].

4.5 Measurement of the caloric curve from cluster photofragmentation

This and the next section are designed to consider recently developed methods for measuring cluster melting temperature and the heat of fusion, in which the clusters melting themselves serve as supersensitive calorimeters to measure energy. These methods use cluster beams and two mass spectrometers: one to select clusters of the desired size, and the other to analyze their fragmentation. The observation of characteristic features in thermal capacity $C(T)$ [see relation (3.1)], apparent from the caloric curve, allows for direct identification of phase transitions in clusters. It is precisely caloric curves for mass-selected sodium clusters that were obtained in Refs [68–71, 176, 182], designed to study their thermal properties. The main idea behind the experiment for measuring the dependence $E(T)$ [68, 70, 176] is as follows (Fig. 13a). A cluster with temperature T_1 is heated to
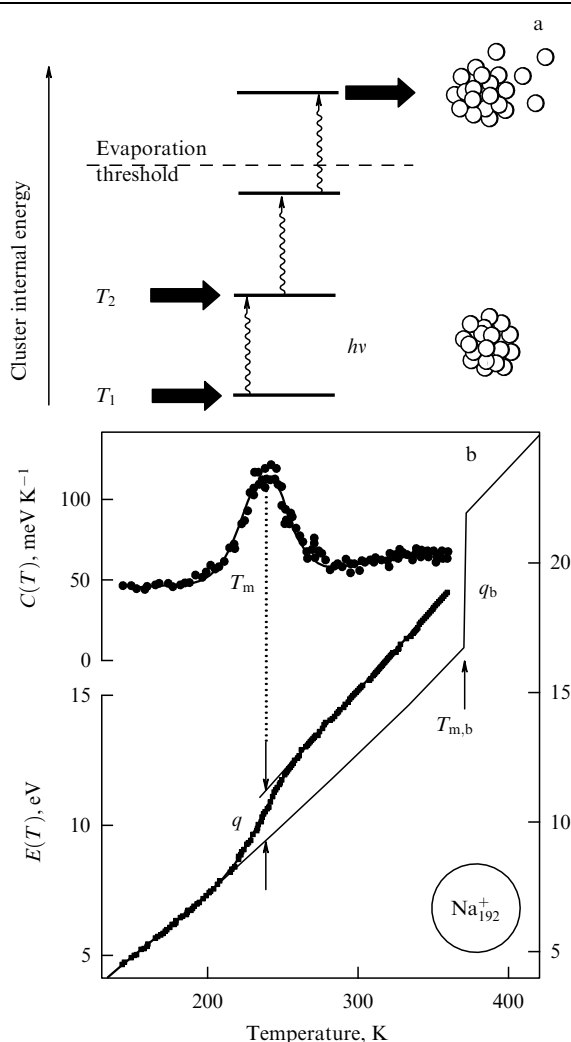
Figure 13. (a) Schematic representation of a cluster laser heating experiment. (b) Temperature dependences of heat capacity and heat of fusion for positively charged sodium clusters containing 192 atoms. Black dots are experimental results. Cluster melting point T_m can be deduced from the $C(T)$ maximum, and latent heat of fusion q from the jump in the caloric curve. The solid line is the caloric curve for bulk matter (normalized to 192 atoms); q_b and $T_{m,b}$ are the corresponding values for bulk matter [69].

temperature T_2 due to absorption of a photon with energy $\delta E = h\nu$. The value of T_2 is then found from measuring the temperature of the cluster source, which increases up to temperature T_2, where the warmed clusters show the same fragmentation pattern (the same mass spectrum) as the laser-heated clusters.

In other words, cluster heat capacity is determined by measuring the temperature dependence of photofragmentation of a mass-selected cluster ion [68, 70, 176]:

$$\mathrm{Na}_N^+(T) + nh\nu \rightarrow \mathrm{Na}_{N-x}^+ + x\mathrm{Na}, \qquad (4.1)$$
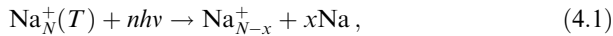
where n is the number of laser photons absorbed sequentially by the cluster ion, and x is the number of neutral sodium atoms emitted from it. The number $x = x(T, n)$ is determined experimentally from the mass spectra of the fragmented cluster ion. The total energy of the warmed and laser-excited cluster ions can be represented as

$$E^*(T, n) = E(T) + nh\nu. \qquad (4.2)$$

There are two ways to increase cluster energy $E(T, n)$ and therefore the number of emitted atoms. First, the *energy* can be directly increased by δE through enlarging the number of absorbed laser photons or their energy. Second, it is possible to heat a cluster prior to laser irradiation and raise its *temperature* by δT. If δE and δT are chosen, such that the cluster emits the same number of atoms, then the following relationship is valid: $E(T + \delta T) = E(T) + \delta E$. In this case, the heat capacity of the cluster can be calculated by replacing differentials in formula (3.1) with finite differences δE and δT.

To sum up, the process of measuring the heat capacity of clusters can be divided into four steps:

(1) Preparation of mass-selected cluster ions with temperature T_1 in a vacuum.

(2) Irradiation of the clusters by laser photons. The absorbed energy ($h\nu = 3.1$ eV $\approx 10^{-18}$ J) relaxes and heats a cluster to temperature T_2 at which it does not yet emit atoms on the time scale of the experiment (for roughly 100 μs). Only after the cluster absorbs a few more (two, as exemplified in Fig. 13a) photons from the same laser pulse does its temperature rise so that it begins to emit atoms by evaporation.

(3) Measurement of cluster ion size distribution following fragmentation with the aid of the second mass spectrometer. This distribution is highly sensitive to the cluster internal energy.

(4) Now, the cluster temperature is increased to T_2, at which absorption of only two laser photons triggers evaporation of the same number of cluster atoms. In so doing, a rise in the energy by δE leads to a rise in temperature by $\delta T = T_2 - T_1$. For relatively small δT, the $\delta E/\delta T$ ratio equals the heat capacity $C(T)$. The melting point of a cluster is the temperature at which the function $C(T)$ reaches its maximum value (Fig. 13b). This method was applied in Refs [68, 70, 71, 176, 182] for a detailed study of heat capacity and heat of fusion of sodium cluster ions. Specifically, it was shown by Schmidt et al. [68] that melting temperature for Na_{139}^+ ions and bulk matter amounts to $T_\mathrm{m} = 267$ K and $T_\mathrm{m} = 371$ K, respectively. The width of the phase transition is 12.6 K. The latent heat of fusion equals 1.98 eV, being significantly lower than for bulk matter (3.69 eV).

4.6 Ion calorimetric method

An ion calorimetric method was developed in Refs [184, 185] to measure the melting temperature and heat of fusion of clusters. The method has its origins in dissociation of cluster ions, induced by multiple collisions with atoms of an inert gas (helium). The approach (Fig. 14) consists in reproducing an identical degree of dissociation of cluster ions (equal internal energy) by alteration of their thermal energy (as a result of heating in the source) and energy acquired in collisions with buffer gas atoms. Measurements were made for aluminium cluster cations with $49-63$ [184] and $63-83$ [185] particles. Cluster heat capacity was studied in a temperature range of $150-1050$ K.

Clusters were generated by laser evaporation of a liquid metal sample in the atmosphere of the buffer gas (helium). The cluster ions thus formed entered the expansion chamber where their temperature underwent variation and stabilization due to collisions with buffer gas atoms. Thereafter, the clusters were mass-selected using a quadrupole mass spectrometer and cluster ions produced were forwarded into a collisional cell containing helium at 1 Torr. Clusters and helium atoms multiply collided in the cell, each collision resulting in the transformation of a small fraction of translational energy into internal energy of the cluster. Given a rather high translational energy of cluster ions entering the cell, some of them were heated to a temperature sufficient for their dissociation. Undissociated parent ions and newly formed ionic fragments were cooled to helium temperature in subsequent collisions, withdrawn from the cell by a weak electric field, and then forwarded to the second quadrupole mass spectrometer for analysis. The fraction of dissociated cluster ions was estimated from the mass spectra.

With a rise in temperature, dissociation of clusters requires less energy due to their higher thermal energy. On reaching the temperature $T_\mathrm{cl} = T_\mathrm{m}$, the amount of energy needed for dissociation sharply decreases on account of the latent heat of fusion [184, 185]. The translational energy $E_\mathrm{tr}^{50\%}$ at which 50% of the ions dissociated was measured in these experiments at different cluster temperatures in the expansion chamber (Fig. 15). This quantity gradually decreased with rising cluster temperature, and a sharp fall in this energy occurred at the melting point. Temperature derivative of the
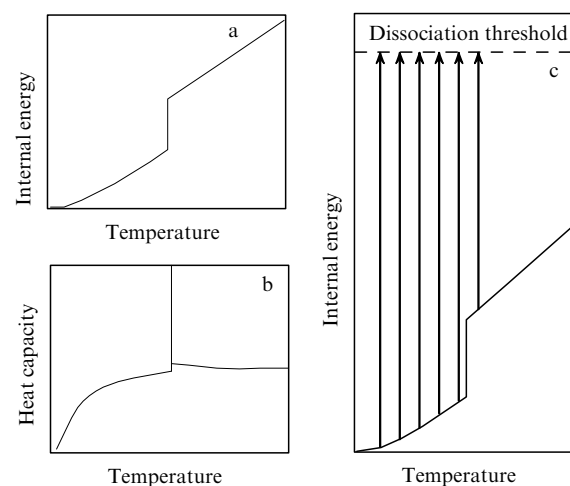
Figure 14. Diagrams illustrating the main principle behind the measurements. (a, b) Temperature dependences of internal energy and heat capacity of a typical crystalline solid. The step in the dependence of internal energy and the jump in the dependence of heat capacity are due to melting. (c) Measurement of the energy necessary to reach the dissociation threshold depending on temperature (arrows); the scheme may be used for measuring the internal energy and determining the melting point [185].
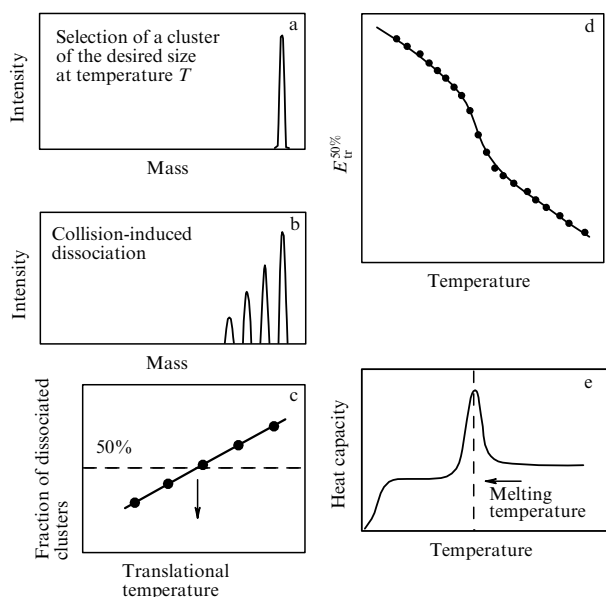
Figure 15. Stepwise process of measuring the heat capacity of isolated cluster ions [185].

dependence $E_{tr}^{50\%}(T)$ obtained is proportional with good accuracy to cluster heat capacity (see Fig. 15). This method was used in Ref. [185] to show evidence that the cluster heat of fusion is approximately 40% lower than that of the respective bulk matter. The melting temperature of clusters undergoes marked fluctuations, depending on their size, and for most of them is significantly lower than for bulk matter. For example, the melting temperature for an Al_{79}^+ cluster ion amounts to 586 K compared with $T_m = 934$ K for the bulk substance. The measured peak width of the temperature dependence of heat capacity for an Al_{79}^+ cluster ion is about 150 K [185]. Consequently, the liquid and solid phases in this cluster coexist within a rather broad (150 K) vicinity of the melting point.

It should be noted in conclusion that the above method of measuring the melting temperature is suitable for clusters dissociating in the liquid phase but not for those that dissociate (sublimate) in the solid phase for $T < T_m$, such as tin clusters.

4.7 Laser methods for melting nanoparticles

Section 4.3 was concerned with data on optical (including laser-aided) methods for observation of phase transitions in clusters, and Section 4.5 described a method for measuring the melting temperature and heat of fusion of Na_N clusters, in which the caloric curve is obtained with the aid of laser radiation. The present section considers in brief a few recently proposed laser-aided techniques for excitation of nanoparticles and observation of their melting. It will be shown that these methods are suitable for observing not only phase transitions in nanoparticles but also a variety of other processes induced after excitation of nanoparticles by intense laser pulses. These observations are possible due to changes in the optical and thermodynamic properties of nanoparticles caused by laser radiation or the manifestation of nonlinear optical effects during phase transitions in particles. Many experiments currently underway make use of pulsed lasers to excite nanoparticles, particularly gold and DNA/Au nanoparticles, and to study various processes in them, including changes in size and shape, ordering, melting, and vaporization [231–241] (see reviews [231, 232] and references cited therein).

Recently, gold and platinum nanoparticles have been used [236, 237] to study the dewetting process which takes place when laser pulses induce melting of nanostructures and cause nanodroplets to detach from the irradiated surface followed by their ballistic jumping to another surface. This process is interesting in that it can be used to deposit nanoparticles onto a new substrate. The results of these studies indicate that this method is suitable to deposit particles of many metals ranging in size from tens to hundreds of nanometers.

The method is based on the following principle [236, 237]. First, flat submicron metal structures are fabricated on a substrate by standard methods, either by colloidal mask lithography or by electron-beam lithography. At the second stage, these microstructured samples are irradiated by intense nanosecond laser pulses sufficient to cause their melting. The second harmonic of an Nd:YAG laser at $\lambda = 532$ nm and a half-height pulse duration of 10 ns was used in experiments. The local liquid volumes formed during melting of the samples show departure from equilibrium with respect to the surface contact angle, equaling 140° for liquid gold meeting the SiO_2 surface [242]; this results in dewetting (Fig. 16a–c) [237]. As a consequence, the liquid material is transported to the center of the metal structure to form a local droplet, which causes vertical displacement of the liquid's center of mass. Then, the liquid droplet leaves the surface due to inertia. This phenomenon has its origins in the conversion of the surface energy of small-sized liquid samples to the kinetic energy of droplets. It was shown in Ref. [237] that the
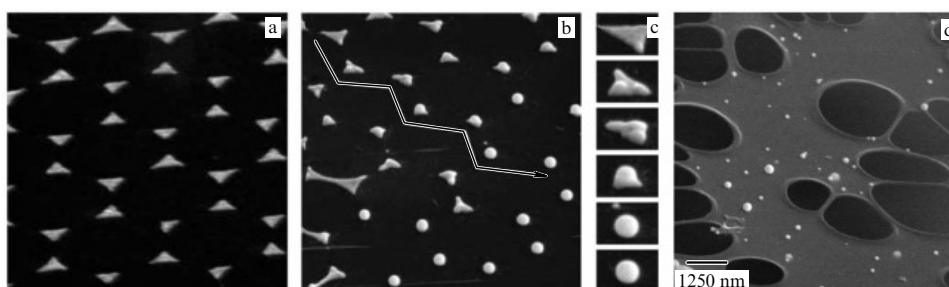

Figure 16. (a) Scanning electron microscope images of triangular gold nanoparticles on an oriented surface of pyrolytic graphite; the nanostructures were produced by colloidal lithography. Substrate tilted. Image size 8×16 µm. (b) The same nanostructures after annealing with a nanosecond laser pulse and resolidification. Along the arrow, the laser fluence and thus the dwell time of the particle's molten state increased. The resulting solid nanostructures therefore represent different stages of the dewetting process (c) [237]. (d) Gold nanoparticles on the carbon grid of a transmission electron microscope [236].

typical speed of the droplets is a few dozen meters per second. Given that a substrate is placed several millimeters apart from the structure being irradiated, the droplets cooled during the flight accumulate on the new substrate. By way of example, Fig. 16d demonstrates gold nanoparticles collected on the carbon grid of a transmission electron microscope [236]. Deposition on new surfaces by this method was also observed for Ag, Ni, and Al nanoparticles [236].

Generation of the second harmonic during irradiation of Ga nanoparticles (inserted into an SiO_x matrix) by femtosecond laser pulses at 800 nm was studied in Ref. [238]. Its signal was shown to be markedly amplified (in both transmitted and reflected light) during phase transitions in nanoparticles. The sample temperature varied from 77 to 320 K. Laser light was absorbed by Ga nanoparticles due to a resonance between the laser second-harmonic radiation and the particle's surface plasmon frequency [243] (Fig. 17). It was expected that the maximum intensity of the laser second harmonic would be observed for a particle radius at which the harmonic is at resonance with the surface plasmon frequency.

It was found in Ref. [238] that the second-harmonic signal displays a strong dependence on nanoparticle size. Figure 18a, b presents size dependences of nonlinear reflection $R_{nl} = I_R(2\omega)/[I_0(\omega)]^2$ and nonlinear transmission $T_{nl} = I_T(2\omega)/[I_0(\omega)]^2$ for nanoparticles. Here, I is the intensity of incident (subscript 0), reflected (subscript R), and transmitted (subscript T) radiation. The second-harmonic signal exhibits quadratic dependence on incident radiation intensity (see inset to Fig. 18a). It can be seen that the signal is strongly dependent on the particle size in a range from 2 to 100 nm. Quantities R_{nl} and T_{nl} behave similarly, depending on particle size. Both dependences have maxima at a particle radius of 20 – 40 nm, confirming the substantial amplification of the second-harmonic signal at resonance with the surface plasmon frequency.

Reference [238] describes hysteresis in the sample temperature dependence of the nonlinear second-harmonic signal (Fig. 19). The hysteresis contour lies in the temperature range from 150 to 270 K. It should be noted that Ga nanoparticles are liquid at 300 K (Fig. 1b). Melting and solidification show
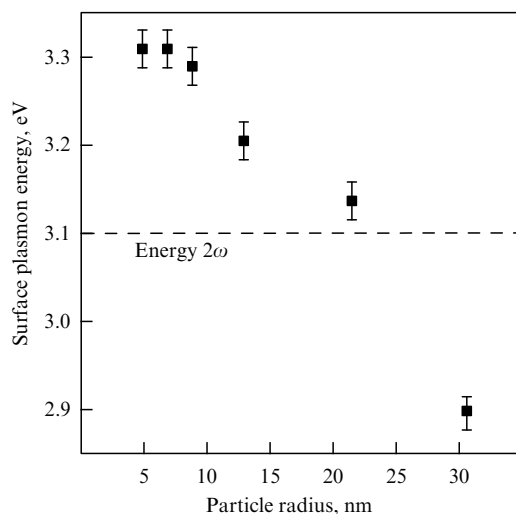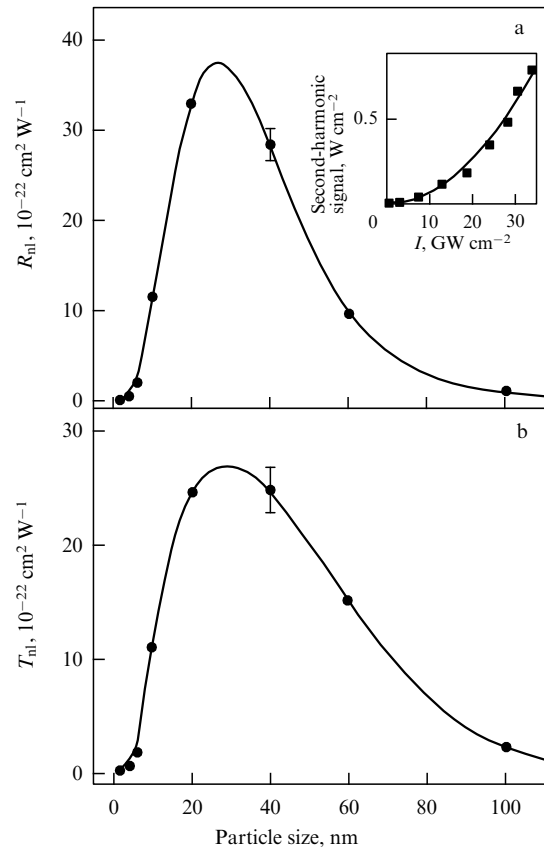
Figure 18. Nonlinear reflection R_{nl} (a) and nonlinear transmission T_{nl} (b) of differently sized Ga nanoparticles inserted into an SiO_x matrix, depending on mean particle radius. Second-harmonic signals were observed at the normal angle of incidence in the transmitted light, and at an angle of 2° in the reflected light. Solid lines are drawn for a better view of the data. Inset: quadratic dependence of the second-harmonic signal on incident radiation intensity [238].

a similar hysteresis for particles with a radius of down to 10 nm. Hysteresis tends to disappear with further decreasing particle size. As the sample temperature rises from 77 to 320 K, the value of T_{nl} grows by 40 – 50%, whereas linear transmission increases by 0.05% at most. This means that the hysteresis cycle illustrated in Fig. 19 is overestimated by roughly two orders of magnitude relative to the linear signal. Hence, the results reported in Ref. [238] are of great interest and importance, especially the observation of hysteresis, for diagnostics of nanoparticles.

Spectroscopic studies of shape variations and solid–liquid phase transitions in gold nanoparticles suspended in water have recently been reported in Refs [239, 240]. It was revealed that relatively large ellipsoid nanoparticles (38.2 nm) transform into smaller spherical particles under the effect of third-harmonic pulses from an Nd:YAG laser ($\lambda = 355$ nm, pulse length 30 ps) [239]. Particle shape and size were determined with a transmission electron microscope. The particles' absorption spectra in a solution were recorded before and after laser irradiation using a multichannel detector (Fig. 20a).

The threshold energy necessary to change the particle's shape was estimated at ~ 40 fJ per particle, which is much smaller than the energy needed to completely melt a particle (67 fJ). These estimates based on accounting for the heat balance and the surface melting model [244] suggest that the particle's temperature following irradiation by a single laser

Figure 17. Plasmon peak position of Ga nanoparticles in the SiO_x matrix, depending on mean particle radius. Experimental points were obtained from the analysis of linear transmission curves. The second-harmonic signal frequency (dashed line) corresponds to 3.09 eV [238].
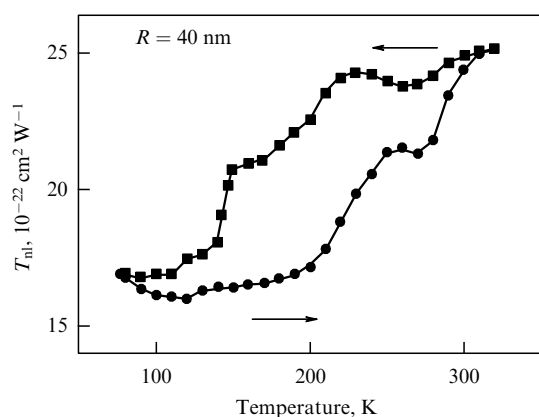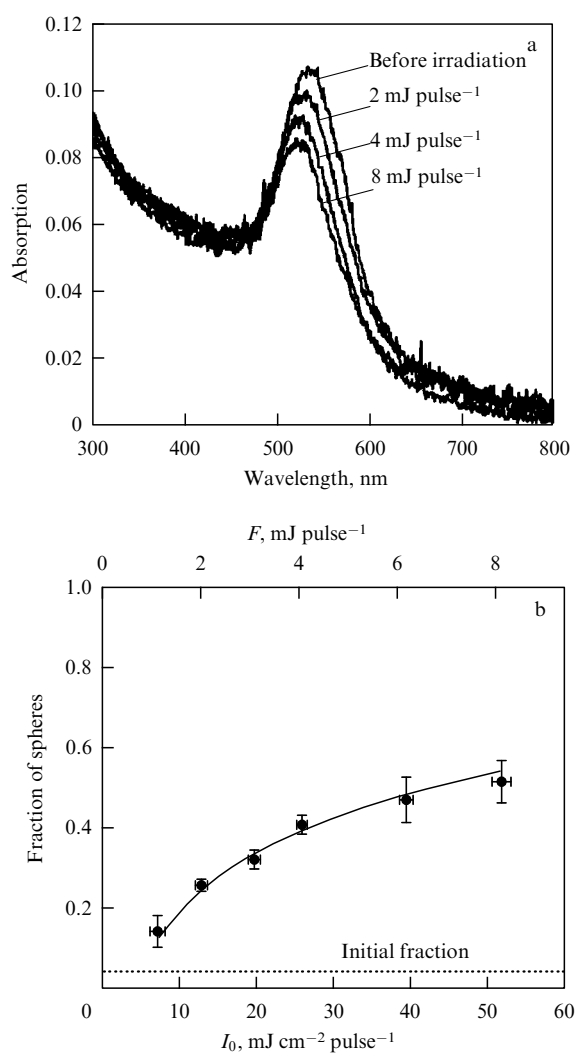
Figure 19. Second-harmonic response of Ga nanoparticles with a mean radius of 40 nm in cooling (squares) and heating (circles) cycles. Sample temperature was measured in a cryostat, where temperature varied from 77 to 320 K at a scanning rate of ~ 2 K min^{-1}. The second-harmonic signal was recorded at the normal incidence angle. Exciting radiation wavelength was 800 nm [238].

Figure 20. (a) Absorption spectra of gold nanoparticles suspended in water before and after irradiation by single laser pulses with a pulse energy of 2, 4, and 8 mJ [239]. (b) Relative number of forming spherical gold particles plotted vs. energy density of an exciting laser pulse [239].

pulse amounts to 940 °C, while the thickness of the liquid surface layer around the particle is ~ 1.4 nm. The shape changes at a temperature approximately 100 °C lower than the melting temperature of bulk gold. The number of spherical particles grows with increasing the energy density of the exciting pulse (Fig. 20b). Cluster transformation on a silicon substrate occurred at 950 °C. Thus, due to surface melting, gold nanoparticles excited by picosecond laser pulses change their shapes at a much lower temperature than the melting temperature of the bulk matter, which is in excellent agreement with theoretical predictions [239, 244].

As shown in Ref. [240], shape variations and a decrease in size of gold nanoparticles in an aqueous solution under the effect of laser pulses were evaluated using the excitation–probing approach. The nanoparticles were excited by picosecond pulses at 355 nm, as described in Ref. [239]. Further changes in nanoparticle absorption spectra were detected using two continuous-wave lasers operated at 488 and 635 nm. The nanoparticle absorption spectra obtained at these wavelengths were used to observe melting and evaporation, which occurred simultaneously with the change in the particles' shape and with the particle's size decreasing.

On a nanosecond time scale at energy densities from 6.3 to 17 mJ cm^{-2}, the nanoparticles produced a pulse bleaching (discoloration) signal at 488 nm, related to their melting. The signal decreased with increasing excitation energy density. At an energy density above 17 mJ cm^{-2}, strong absorption at both wavelengths occurred, which was attributable to the evaporation of gold nanoparticles. The absorption signal died out faster than in 5 ns (resolving time scale of the detecting system). Thereafter, absorption at $\lambda = 635$ nm increased with a time constant of around 1 μs but did not change at $\lambda = 488$ nm. The authors argue that a rise in absorption at 635 nm was due to the formation of small gold nanoparticles as a result of diminution of the starting particle size and subsequent clustering of evaporated atoms.

To conclude this section, it is worth mentioning the interesting results obtained by Plech et al. [241]. Gold nanoparticles 35 nm in size suspended in water were excited by femtosecond (150 fs) laser pulses at 800 nm. Nanoparticles and solvent (water) particles were identified after excitation by the X-ray pulse scattering method [245]. It was revealed that the ultrafast femtosecond excitation of gold nanoparticles causes phase transition in the surrounding water layers (evaporation and bubble formation). As a result, a microshock wave is generated near the nanoparticles. The expansion zone in the vicinity of a nanoparticle (bubble) collapses within a few nanoseconds. Simultaneously, gold nanoparticles melt and undergo fragmentation. Small fragments form clusters on the microsecond time scale, giving rise to new particles around 9 Å in size. In other words, it was shown in Ref. [241] that the excitation of gold nanoparticles suspended in water by femtosecond laser pulses creates within nanoseconds extreme thermodynamic conditions. These conditions are of interest and attractive for the investigation of fast nonequilibrium processes. It is also noteworthy that the aforementioned extreme conditions have a strong effect on the structural changes in the nanoparticles themselves and thereby influence the phase transition and fragmentation.

Thus, the data considered in this section indicate that the excitation of nanoparticles by laser pulses induces solid–liquid phase transitions in them and may be used to diagnose particles and various processes in them.

5. Conclusions

The results of research show that cluster (nanoparticle) temperature is an important physical characteristic determining many properties of clusters, such as polarizability, the magnetic moment, the ionization potential, the optical response, the structure, the configuration, and the phase state. Physicochemical processes involving clusters and cluster beams, including fragmentation (evaporation) and chemical reaction rates, fragmentation channels, energy relaxation rates and channels, greatly depend on cluster temperature.

The upper limiting temperature of large van der Waals clusters generated in nozzle sources, stabilized by evaporation, depends on the interatomic (intermolecular) binding energy inside clusters. Their temperature can be estimated from the energy of sublimation and vaporization heat of the respective bulk matter constituting clusters. At the same time, the use of a carrier gas with low binding energy in nozzle sources makes it possible to produce clusters with the much lower temperature than that determined by the binding energy.

The solid–liquid phase transition in clusters (nanoparticles) is more complicated than an analogous transition in the macroscopic substance, its main distinctive features being coexistence of the two phases in a certain borderline temperature region and the possibility of existence of negative heat capacity of a cluster near the melting point. In both cases, the phase transition reflects configuration excitation of the system considered in the framework of the void concept.

The melting temperature and heat of fusion of clusters decrease as their size decreases. Small clusters ($N \leqslant 200$) are characterized by a strong size dependence of both temperature and heat of fusion that has a nonmonotonic (oscillatory) character due to the equally strong size dependence of the cluster structure. Clusters with completely filled electronic and (or) atomic shells ('magic' clusters) have a much higher melting temperature and heat of fusion than those with incompletely filled shells.

The available tools for the measurement of cluster melting temperature (optical, calorimetric, and mass-spectrometric methods, electron diffraction) permit determining cluster temperature with a high degree of accuracy. Calorimetric methods and ion mass spectrometry enable measuring both the melting temperature and heat of fusion of clusters (nanoparticles) using the clusters themselves as highly sensitive calorimeters.

Laser-aided methods of nanoparticle excitation and melting are utilized for diagnostic purposes and the observation of solid–liquid phase transitions in nanoparticles. Moreover, they yield information about many processes in nanoparticles undergoing irradiation at different wavelengths and intensities. However, these techniques are unsuitable for the direct determination of the melting temperature and heat of fusion of nanoparticles. These characteristics can be estimated indirectly from the particle size, absorption and scattering coefficients of nanoparticles at the exciting radiation wavelength. The data obtained thus far give reason to believe that rapid progress in cluster (nanoparticle) research with the aid of laser pulses will soon bring about new methods for the measurement of cluster melting temperature and heat of fusion. The most promising technique in this context is laser spectroscopy of composite clusters, analogous to the methods described in Section 4.3 [220, 228].

To conclude, studies of cluster melting temperature are important in relation to the superfluid hydrogen problem. In 1972, V L Ginzburg and A A Sobyanin demonstrated [246] that liquid para-hydrogen could pass to the superfluid state at temperature $T \approx 6$ K if it did not freeze at $T = 13.6$ K. This finding gave incentive to the search for the metastable state of liquid para-hydrogen with a relatively low freezing temperature. In small clusters, the temperature of freezing is very low, and spectroscopic studies showed that hydrogen clusters of $N \leqslant 50$ molecules formed in a supersonic gas jet are liquid rather than solid [247]. This was established on the base of spectroscopic observations. The spectroscopic characteristics of CO chromophore molecules introduced into (para-$H_2)_N$ clusters containing $N = 7-17$ hydrogen molecules give evidence of dissipationless sliding during CO rotation inside the clusters [248]. This suggests the superfluid nature of small para-hydrogen clusters in analogy with superfluid ^{4}He clusters [30 – 36, 41, 249].

References

1. Pauly H *Atom, Molecule, and Cluster Beams* Vol. 2 *Cluster Beams, Fast and Slow Beams, Accessory Equipment, and Applications* (Berlin: Springer, 2000)
2. Jena P, Khanna S N, Rao B K (Eds) *Physics and Chemistry of Finite Systems: From Clusters to Crystals* (Dordrecht: Kluwer Acad. Publ., 1992)
3. de Heer W A *Rev. Mod. Phys.* **65** 611 (1993)
4. Billups W E, Ciufolini M A (Eds) *Buckminsterfullerenes* (New York: VCH, 1993)
5. Haberland H (Ed.) *Clusters of Atoms and Molecules*: *Theory, Experiment, and Clusters of Atoms* (Heidelberg: Springer-Verlag, 1994)
6. Klabunde K J *Free Atoms, Clusters, and Nanoscale Particles* (San Diego: Academic Press, 1994)
7. Smirnov B M *Usp. Fiz. Nauk* **164** 1165 (1994) [*Phys. Usp.* **37** 1079 (1994)]
8. Eletskii A V, Smirnov B M *Usp. Fiz. Nauk* **165** 977 (1995) [*Phys. Usp.* **38** 935 (1995)]
9. Kondow T, Kaya K, Terasaki A (Eds) *Structures and Dynamics of Clusters* (Tokyo: Universal Academy Press, 1996)
10. Martin T P (Ed.) *Large Clusters of Atoms and Molecules* (Dordrecht: Kluwer Acad., 1996)
11. Yoshimura S, Chang R P H *Supercarbon* (Heidelberg: Springer, 1998)
12. Hirsch A *Fullerenes and Related Structures* (Heidelberg: Springer-Verlag, 1998)
13. Smirnov B M *Clusters and Small Particles*: *in Gases and Plasmas* (New York: Springer, 2000)
14. Alivisatos A P *J. Phys. Chem.* **100** 13226 (1996)
15. Castleman A W (Jr.), Bowen K H (Jr.) *J. Phys. Chem.* **100** 12911 (1996)
16. Eletskii A V *Usp. Fiz. Nauk* **167** 945 (1997) [*Phys. Usp.* **40** 899 (1997)]
17. Christen W, Even U *J. Phys. Chem. A* **102** 9420 (1998)
18. Herschbach D *Rev. Mod. Phys.* **71** S411 (1999)
19. Smalley R E *Rev. Mod. Phys.* **69** 723 (1997); *Usp. Fiz. Nauk* **168** 323 (1998)
20. Curl R F *Rev. Mod. Phys.* **69** 691 (1997); *Usp. Fiz. Nauk* **168** 331 (1998)
21. Kroto H *Rev. Mod. Phys.* **69** 703 (1997); *Usp. Fiz. Nauk* **168** 343 (1998)

22. Rakov E G *Usp. Khim.* **69** 41 (2000) [*Russ. Chem. Rev.* **69** 35 (2000)]
23. Perez A et al. *J. Phys. D* **30** 709 (1997)
24. Krainov V P, Smirnov M B *Usp. Fiz. Nauk* **170** 969 (2000) [*Phys. Usp.* **43** 901 (2000)]
25. Smirnov B M *Usp. Fiz. Nauk* **171** 1291 (2001) [*Phys. Usp.* **44** 1229 (2001)]
26. Krainov V P, Smirnov M B *Phys. Rep.* **370** 237 (2002)
27. Smirnov B M *Usp. Fiz. Nauk* **173** 609 (2003) [*Phys. Usp.* **46** 589 (2003)]
28. Ditmire T et al. *Phys. Rev. A* **53** 3379 (1996)
29. Zweiback J et al. *Phys. Plasmas* **9** 3108 (2002)
30. Kwon Y et al. *J. Chem. Phys.* **113** 6469 (2000)
31. Northby J A *J. Chem. Phys.* **115** 10065 (2001)
32. Callegari C et al. *J. Chem. Phys.* **115** 10090 (2001)
33. Stienkemeier F, Vilesov A F *J. Chem. Phys.* **115** 10119 (2001)
34. Toennies J P, Vilesov A F, Whaley K B *Phys. Today* **54** (2) 31 (2001)
35. Toennies J P, Vilesov A F *Angew. Chem. Int. Ed.* **43** 2622 (2004)
36. Makarov G N *Usp. Fiz. Nauk* **174** 225 (2004) [*Phys. Usp.* **47** 217 (2004)]
37. Yamada I, Toyoda N *Nucl. Instrum. Meth. Phys. Res. B* **232** 195 (2005)
38. Berry R S, Smirnov B M *Usp. Fiz. Nauk* **175** 367 (2005) [*Phys. Usp.* **48** 345 (2005)]
39. Makarov G N *Usp. Fiz. Nauk* **176** 121 (2006) [*Phys. Usp.* **49** 117 (2006)]
40. Eletskii A V *Usp. Fiz. Nauk* **177** 233 (2007) [*Phys. Usp.* **50** 225 (2007)]
41. Makarov G N *Usp. Fiz. Nauk* **176** 1155 (2006) [*Phys. Usp.* **49** 1131 (2006)]
42. Krainov V P, Smirnov B M, Smirnov M B *Usp. Fiz. Nauk* **177** 953 (2007) [*Phys. Usp.* **50** 907 (2007)]
43. Makarov G N *Usp. Fiz. Nauk* **178** 337 (2008) [*Phys. Usp.* **51** 319 (2008)]
44. Kresin V Z, Ovchinnikov Yu N *Usp. Fiz. Nauk* **178** 449 (2008) [*Phys. Usp.* **51** 427 (2008)]
45. Berry R S, Smirnov B M *Usp. Fiz. Nauk* **179** 147 (2009) [*Phys. Usp.* **52** 137 (2009)]
46. Makarov G N *Usp. Fiz. Nauk* **179** 487 (2009) [*Phys. Usp.* **52** 461 (2009)]
47. Ginzburg V L *Usp. Fiz. Nauk* **169** 419 (1999) [*Phys. Usp.* **42** 353 (1999)]
48. Ginzburg V L *Usp. Fiz. Nauk* **177** 346 (2007) [*Phys. Usp.* **50** 332 (2007)]
49. Rubahn H-G *Nanophysik und Nanotechnologie* (Stuttgart: Teubner Verlag, 2002)
50. Edelstein A S, Cammarata R C (Eds) *Nanomaterials: Synthesis, Properties, and Applications* (Bristol: Institute of Physics Publ., 1996)
51. Moro R et al. *Science* **300** 1265 (2003)
52. Moro R et al. *Phys. Rev. Lett.* **93** 086803 (2004)
53. Andersen K E et al. *Phys Rev. B* **73** 125418 (2006)
54. Xu X et al. *Phys Rev. B* **75** 085429 (2007)
55. Siegel R W, Hu E, Roco M C (Eds) *Nanostructure Science and Technology* (Dordrecht: Kluwer Acad. Publ., 1999)
56. Schmid G (Ed.) *Nanoparticles: From Theory to Application* (Weinheim: Wiley-VCH, 2004)
57. Renn O, Roco M C *J. Nanopart. Res.* **8** 153 (2006)
58. Barnett R N, Landman U *Nature* **387** 788 (1997)
59. Berry R S, Smirnov B M *Zh. Eksp. Teor. Fiz.* **117** 562 (2000) [*JETP* **90** 491 (2000)]
60. Berry R S, Smirnov B M *Zh. Eksp. Teor. Fiz.* **125** 414 (2004) [*JETP* **98** 366 (2004)]
61. Landau L D, Lifshitz E M *Statisticheskaya Fizika* (Statistical Physics) Pt. 1 (Moscow: Nauka, 1976) [Translated into English, Pt. 1 (Oxford: Pergamon Press, 1980)]
62. Bixon M, Jortner J *J. Chem. Phys.* **91** 1631 (1989)
63. Labastie P, Whetten R L *Phys. Rev. Lett.* **65** 1567 (1990)
64. Wales D J *Mol. Phys.* **78** 151 (1993)
65. Wales D J, Berry R S *Phys. Rev. Lett.* **73** 2875 (1994)
66. Umirzakov I H *Phys. Rev. E* **60** 7550 (1999)
67. Mülken O, Stamerjohanns H, Borrmann P *Phys. Rev. E* **64** 047105 (2001)
68. Schmidt M et al. *Phys. Rev. Lett.* **79** 99 (1997)
69. Schmidt M et al. *Nature* **393** 238 (1998)
70. Schmidt M et al. *Phys. Rev. Lett.* **86** 1191 (2001)
71. Schmidt M et al. *Phys. Rev. Lett.* **87** 203402 (2001)
72. Gobet F et al. *Phys. Rev. Lett.* **89** 183403 (2002)
73. Reyes-Nava J A, Garzón I L, Michaelian K *Phys. Rev. B* **67** 165401 (2003)
74. Harms J et al. *J. Mol. Spectrosc.* **185** 204 (1996)
75. Brink D M, Stringari S *Z. Phys. D* **15** 257 (1990)
76. Vostrikov A A, Dubov D Yu, Agarkov A A *Pis'ma Zh. Eksp. Teor. Fiz.* **63** 915 (1996) [*JETP Lett.* **63** 963 (1996)]
77. Agarkov A A et al. *Eur. Phys J. D* **9** 331 (1999)
78. Vostrikov A A, Agarkov A A, Dubov D Yu *Zh. Tekh. Fiz.* **70** (7) 102 (2000) [*Tech. Phys.* **45** 915 (2000)]
79. Vostrikov A A, Dubov D Yu, Agarkov A A *Teplofiz. Vys. Temp.* **39** 26 (2001) [*High Temp.* **39** 22 (2001)]
80. Foltin M et al. *J. Chem. Phys.* **98** 9624 (1993)
81. Wan Z et al. *J. Chem. Phys.* **99** 5858 (1993)
82. Wan Z, Christian J F, Anderson S L *J. Chem. Phys.* **96** 3344 (1992)
83. Rohlfing E A *J. Chem. Phys.* **89** 6103 (1988)
84. Mitzner R, Campbell E E B *J. Chem. Phys.* **103** 2445 (1995)
85. Heszler P, Carlsson J O, Demirev P *J. Chem. Phys.* **107** 10440 (1997)
86. Frenzel U et al. *Z. Phys. D* **40** 108 (1997)
87. Frenzel U et al. *Surf. Rev. Lett.* **3** 505 (1996)
88. Heszler P, Carlsson J O, Demirev P *Phys. Rev. B* **53** 12541 (1996)
89. Mitzner R, Campbell E E B *Surf. Rev. Lett.* **3** 759 (1996)
90. Campbell E E B et al. *Phys. Rev. Lett.* **70** 263 (1993)
91. Schulte J et al. *Phys. Lett. A* **198** 51 (1995)
92. Schmidt R, Seifert G, Lutz H O *Phys. Lett. A* **158** 231 (1991)
93. Seifert G, Schmidt R, Lutz H O *Phys. Lett. A* **158** 237 (1991)
94. Farizon B, Farizon M, Gaillard M J *Int. J. Mass Spectrom.* **192** 259 (1999)
95. Campbell E E B et al. *C.R. Physique* **3** 341 (2002)
96. Smirnov B M *Pis'ma Zh. Eksp. Teor. Fiz.* **81** 8 (2005) [*JETP Lett.* **81** 6 (2005)]
97. Bulgac A *Czech. J. Phys.* **48** 697 (1998)
98. Li Y, Blaisten-Barojas E, Papaconstantopoulos D A *Phys. Rev. B* **57** 15519 (1998)
99. Bréchignac C et al. *Phys. Rev. Lett.* **89** 183402 (2002)
100. Bréchignac C et al. *Phys. Rev. A* **68** 063202 (2003)
101. Ho J et al. *J. Chem. Phys.* **99** 140 (1993)
102. Boyukata M et al. *Int. J. Mod. Phys. C* **16** 295 (2005)
103. Gée C et al. *J. Phys. Chem.* **100** 13421 (1996)
104. Gée C et al. *J. Chem. Phys.* **107** 4194 (1997)
105. Lugovoj E, Toennies J P, Vilesov A *J. Chem. Phys.* **112** 8217 (2000)
106. Lallement A et al. *Chem. Phys. Lett.* **189** 182 (1992)
107. Yamaguchi N et al. *Thin Solid Films* **345** 34 (1999)
108. Yamaguchi N, Terashima K, Yoshida T *J. Mater. Sci. Lett.* **17** 2067 (1998)
109. Farges J et al. *Surf. Sci.* **106** 95 (1981)
110. Gspann J *Z. Phys. D* **3** 143 (1986)
111. Gspann J, in *Physics of Electronic and Atomic Collisions* (Ed. S Datz) (Amsterdam: North-Holland, 1982) p. 79
112. Frenkel J *Kineticheskaya Teoriya Zhidkostei* (Kinetic Theory of Liquids) (Moscow – Leningrad: Izd. AN SSSR, 1945) [Translated into English (Oxford: The Univ. Press, 1946)]
113. Klein M L, Venables J A (Eds) *Rare Gas Solids* Vol. II (London: Academic Press, 1977)
114. Farges J *J. Cryst. Growth* **31** 79 (1975)
115. Farges J et al. *J. Physique* **38** (C2-7) 47 (1977)
116. Torchet G, Docteures-Sciences Thesis (Paris: Paris Univ., 1978)
117. Robinson P J, Holbrook K A *Unimolecular Reactions* (London: Wiley, 1972) [Translated into Russian (Moscow: Mir, 1975)]
118. Eyring H, Lin S H, Lin S M *Basic Chemical Kinetics* (New York: Wiley, 1980)
119. Klots C E *Z. Phys D* **5** 83 (1987)
120. Klots C E *Nature* **327** 222 (1987)
121. Klots C E *J. Phys Chem.* **92** 5864 (1988)
122. Hansen K, Campbell E E B *Int. J. Mass Spectrom.* **233** 215 (2004)
123. Lide D R (Ed.) *CRC Handbook of Chemistry and Physics* 74th ed. (Boca Raton: CRC Press, 1993 – 1994)
124. Torchet G et al. *J. Chem. Phys.* **79** 6196 (1983)
125. Valente E J, Bartell L S *J. Chem. Phys.* **79** 2683 (1983)
126. Valente E J, Bartell L S *J. Chem. Phys.* **80** 1451 (1984)
127. Natanson G, Amar F, Berry R S *J. Chem. Phys.* **78** 399 (1983)

128. Jellinek J, Beck T L, Berry R S *J. Chem. Phys.* **84** 2783 (1986)
129. Beck T L, Jellinek J, Berry R S *J. Chem. Phys.* **87** 545 (1987)
130. Davis H L, Jellinek J, Berry R S *J. Chem. Phys.* **86** 6456 (1987)
131. Berry R S, Jellinek J, Natanson G *Phys. Rev. A* **30** 919 (1984)
132. Beck T L, Berry R S *J. Chem. Phys.* **88** 3910 (1988)
133. Wales D J, Berry R S *J. Chem. Phys.* **92** 4283 (1990)
134. Berry R S *Chem. Rev.* **93** 2379 (1993)
135. Berry R S *Nature* **393** 212 (1998)
136. Berry R S, in *Theory of Atomic and Molecular Clusters* (Ed. J Jellinek) (Berlin: Springer, 1999) p. 1
137. Cheng H-P, Berry R S *Phys. Rev. A* **45** 7969 (1992)
138. Kunz R E, Berry R S *Phys. Rev. Lett.* **71** 3987 (1993)
139. Kunz R E, Berry R S *Phys. Rev. E* **49** 1895 (1994)
140. Wales D J *Chem. Phys. Lett.* **166** 419 (1990)
141. Wales D J *Mol. Phys.* **78** 151 (1993)
142. Wales D J, Ohmine I *J. Chem. Phys.* **98** 7245 (1993)
143. Wales D J *Adv. Chem. Phys.* **115** 1 (2000)
144. Wales D J *Energy Landscapes* (Cambridge: Cambridge Univ. Press, 2003)
145. Berry R S, Wales D J *Phys. Rev. Lett.* **63** 1156 (1989)
146. Wales D J, Berry R S *J. Chem. Phys.* **92** 4473 (1990)
147. Berry R S, Smirnov B M *Zh. Eksp. Teor. Fiz* **122** 298 (2002) [*JETP* **95** 255 (2002)]
148. Berry R S, Smirnov B M *Zh. Eksp. Teor. Fiz.* **127** 1282 (2005) [*JETP* **100** 1129 (2005)]
149. Berry R S et al. *Adv. Chem. Phys.* **90** 75 (1988)
150. Briant C L, Burton J J *J. Chem. Phys.* **63** 2045 (1975)
151. Damgaard Kristensen W, Jensen E J, Cotterill M R J *J. Chem. Phys.* **60** 4161 (1974)
152. Etters R D, Kaelberer J B *Phys. Rev. A* **11** 1068 (1975)
153. Kaelberer J B, Etters R D *J. Chem. Phys.* **66** 3233 (1977)
154. Etters R D, Kaelberer J B *J. Chem. Phys.* **66** 5112 (1977)
155. Hoare M R, Pal P *Adv. Phys.* **20** 161 (1971); **24** 645 (1975)
156. Hoare M R *Adv. Phys.* **40** 49 (1979)
157. Ball K D, Berry R S *J. Chem. Phys.* **111** 2060 (1999)
158. Stillinger F H, Weber T A *Phys. Rev. A* **25** 978 (1982)
159. Corti D S et al. *Phys. Rev. E* **55** 5522 (1997)
160. Stillinger F H, Weber T A *Phys. Rev. A* **28** 2408 (1983)
161. Becker O M, Karplus M *J. Chem. Phys.* **106** 1495 (1997)
162. Komatsuzaki T, Berry R S *J. Chem. Phys.* **110** 9160 (1999)
163. Vekhter B et al. *J. Chem. Phys.* **106** 4644 (1997)
164. Kubo R *Statistical Mechanics* (Amsterdam: North-Holland, 1965) [Translated into Russian (Moscow: Mir, 1967)]
165. Bragg W, Williams H J *Proc. R. Soc. London Ser. A* **145** 699 (1934)
166. Ziman J M *Models of Disorder* (Cambridge: Cambridge Univ. Press, 1979) [Translated into Russian (Moscow: Mir, 1982)]
167. Smirnov B M *Statistical Physics and Kinetic Theory of Atomic Systems* (Moscow: IVT RAN, 2001)
168. Reiss H, Frisch H L, Lebowitz J L *J. Chem. Phys.* **31** 369 (1959)
169. Lindemann F A *Z. Phys.* **11** 609 (1910)
170. Hansen J-P, Verlet L *Phys. Rev.* **184** 151 (1969)
171. Zhou Y et al. *J. Chem. Phys.* **116** 2323 (2002)
172. Pawlow P *Z. Phys. Chem.* **65** 1,545 (1909)
173. Takagi M *J. Phys. Soc. Jpn.* **9** 359 (1954)
174. Berry R S *Sci. Am.* **263** (2) 50 (1990)
175. Martin T P et al. *J. Chem. Phys.* **100** 2322 (1994)
176. Haberland H et al. *Phys. Rev. Lett.* **94** 035701 (2005)
177. Garrigos R, Cheyssac P, Kofman R *Z. Phys. D* **12** 497 (1989)
178. Lai S L et al. *Phys. Rev. Lett.* **77** 99 (1996)
179. Martin T P *Phys. Rep.* **273** 199 (1996)
180. Jortner J et al., in *The Chemical Physics of Atomic and Molecular Clusters: Proc. of the Intern. School of Physics 'Enrico Fermi'. Course LI* (New York: Academic Press, 1971) p. 73
181. Berry R S, in *Clusters of Atoms and Molecules: Theory, Experiment, and Clusters of Atoms* (Ed. H Haberland) (Berlin: Springer-Verlag, 1994) Ch. 2.8
182. Schmidt M et al. *Phys. Rev. Lett.* **90** 103401 (2003)
183. Krishnamurty S et al. *Phys. Rev. B* **73** 045406 (2006)
184. Breaux G A et al. *Phys. Rev. Lett.* **94** 173401 (2005)
185. Neal C M, Starace A K, Jarrold M F *J. Am. Soc. Mass Spectrom.* **18** 74 (2007)
186. Bachels T, Güntherodt H-J, Schäfer R *Phys. Rev. Lett.* **85** 1250 (2000)
187. Smirnov B M *Usp. Fiz. Nauk* **177** 369 (2007) [*Phys. Usp.* **50** 354 (2007)]
188. Ercolessi F, Andreoni W, Tosatti E *Phys. Rev. Lett.* **66** 911 (1991)
189. Ju N, Bulgac A *Phys. Rev. B* **48** 2721 (1993)
190. Smirnov B M *Phys. Scripta* **50** 427 (1994)
191. Hervieux P A, Gross D H E *Z. Phys. D* **33** 295 (1995)
192. Calvo F, Spiegelmann F *J. Chem. Phys.* **112** 2888 (2000)
193. Aguado A et al. *J. Phys. Chem. B* **105** 2386 (2001)
194. Berry R S, Smirnov B M *J. Chem. Phys.* **118** 5979 (2003)
195. Ding F, Rosén A, Bolton K *Phys. Rev. B* **70** 075416 (2004)
196. Teng Y et al. *J. Phys. Chem. B* **111** 2309 (2007)
197. Duan H et al. *Chem. Phys.* **333** 57 (2007)
198. Zhukov A V, Kraynyukova A, Cao J *Phys. Lett. A* **364** 329 (2007)
199. Shvartsburg A A, Jarrold M F *Phys. Rev. Lett.* **85** 2530 (2000)
200. Joshi K, Kanhere D G, Blundell S A *Phys. Rev. B* **66** 155329 (2002)
201. Joshi K, Kanhere D G, Blundell S A *Phys. Rev. B* **67** 235413 (2003)
202. Breaux G A et al. *Phys. Rev. Lett.* **91** 215508 (2003)
203. Hu W et al. *Eur. Phys. J. B* **45** 547 (2005)
204. Wang L et al. *Acta Phys. Chim. Sinica* **17** (12) 1097 (2001)
205. Lozovik Y E, Popov A M *Mol. Mater.* **13** 213 (1997)
206. Lozovik Yu E, Popov A M *Chem. Phys. Lett.* **328** 355 (2000)
207. Cheng D, Huang S, Wang W *Phys. Rev. B* **74** 064117 (2006)
208. Aguado A, López J M, Núñez S *Comput. Mater. Sci.* **35** 174 (2006)
209. Joshi K, Kanhere D G *J. Chem. Phys.* **119** 12301 (2003)
210. Mottet C et al. *Ann. Chem. Sci. Mater.* **30** (3) 303 (2005)
211. Antonelli A, Khanna S N, Jena P *Phys. Rev. B* **48** 8263 (1993)
212. Kuo C-L, Clancy P *J. Phys. Chem. B* **109** 13743 (2005)
213. Lu H M, Han F Q, Mong X K *J. Phys. Chem. B* **112** 9444 (2008)
214. Moitra A et al. *J. Phys. D* **41** 185406 (2008)
215. Manninen K, Rytkönen A, Manninen M *Eur. Phys. J. D* **29** 39 (2004)
216. Sun J, Simon S L *Thermochim. Acta* **463** 32 (2007)
217. Pacheco J M, Schöne W-D *Phys. Rev. Lett.* **79** 4986 (1997)
218. Ellert C et al. *Phys. Rev. Lett.* **75** 1731 (1995)
219. Reiners Th et al. *Chem. Phys. Lett.* **215** 357 (1993)
220. Hahn M Y, Whetten R L *Phys. Rev. Lett.* **61** 1190 (1988)
221. Zabel T, Garcia M E, Bennemann K H *Eur. Phys. J. D* **7** 219 (1999)
222. Cheng H-C et al. *Israel J. Chem.* **39** 231 (1999)
223. Wang Y-S et al. *J. Am. Chem. Soc.* **120** 8777 (1998)
224. Jiang J-C et al. *J. Am. Chem. Soc.* **122** 1398 (2000)
225. Thompson J M, Bulgac A *Z. Phys. D* **40** 462 (1997)
226. Selby K et al. *Phys. Rev. B* **43** 4565 (1991)
227. Schmidt M et al. *Phys. Rev. B* **59** 10970 (1999)
228. Even U, Ben-Horin N, Jortner J *Phys. Rev. Lett.* **62** 140 (1989)
229. Stuckless J T, Frei N A, Campbell C T *Rev. Sci. Instrum.* **69** 2427 (1998)
230. Binnewies M, Milke E *Thermochemical Data of Elements and Compounds* (Weinheim: Wiley-VCH, 1999) p. 871
231. Link S, El-Sayed M A *Int. Rev. Phys. Chem.* **19** 409 (2000)
232. Sun Y, Harris N C, Kiang C-H *Plasmonics* **2** 193 (2007)
233. Pedraza A J et al. *J. Mat. Res.* **17** 2815 (2002)
234. Park S Y et al. *J. Phys. Chem. B* **110** 12673 (2006)
235. Sugiyama M, Okazaki H, Koda S *Jpn. J. Appl. Phys.* **41** 4666 (2002)
236. Boneberg J et al. *Appl. Phys. A* **93** 415 (2008)
237. Habenicht A et al. *Science* **309** 2043 (2005)
238. Malvezzi A M et al. *Phys. Rev. Lett.* **89** 087401 (2002)
239. Inasawa S, Sugiyama M, Yamaguchi Y *J. Phys. Chem. B* **109** 3104 (2005)
240. Inasawa S et al. *J. Phys. Chem.* **110** 3114 (2006)
241. Plech A et al. *Chem. Phys. Lett.* **401** 565 (2005)
242. Naidich J V, in *Progress in Surface and Membrane Science* Vol. 14 (Eds D A Cadenhead, J F Danielli) (New York: Academic Press, 1981) p. 353
243. Tognini P et al. *J. Non-Cryst. Solids* **249** 117 (1999)
244. Kofman R et al. *Surf. Sci.* **303** 231 (1994)
245. Plech A et al. *Phys. Rev. Lett.* **92** 125505 (2004)
246. Ginzburg V L, Sobyanin A A *Pis'ma Zh. Eksp. Teor. Fiz.* **15** 343 (1972) [*JETP Lett.* **15** 242 (1972)]
247. Tejeda G et al. *Phys. Rev. Lett.* **92** 223401 (2004)
248. Moroni S et al. *J. Chem. Phys.* **122** 094314 (2005)
249. Dumesh B S, Surin L A *Usp. Fiz. Nauk* **176** 1137 (2006) [*Phys. Usp.* **49** 1113 (2006)]